Non-Markovian quantum fluctuations and superradiance near a photonic band edge

Nipun Vats and Sajeev John

Department of Physics, University of Toronto, 60 St. George Street, Toronto, Ontario, Canada M5S 1A7

We discuss a point model for the collective emission of light from N two-level atoms in a photonic band-gap material, each with an atomic resonant frequency near the edge of the gap. In the limit of a low initial occupation of the excited atomic state, our system is shown to possess atomic spectra and population statistics that are radically different from free space. For a high initial excited-state population, mean-field theory suggests a fractionalized inversion and a macroscopic polarization for the atoms in the steady state, both of which can be controlled by an external dc field. This atomic steady state is accompanied by a nonzero expectation value of the electric field operators for field modes located in the vicinity of the atoms. The nature of homogeneous broadening near the band edge is shown to differ markedly from that in free space due to non-Markovian memory effects in the radiation dynamics. Non-Markovian vacuum fluctuations are shown to yield a partially coherent steady-state polarization with a random phase. In contrast with the steady state of a conventional laser, near a photonic band edge this coherence occurs as a consequence of photon localization in the absence of a conventional cavity mode. We also introduce a classical stochastic function with the same temporal correlations as the electromagnetic reservoir, in order to stochastically simulate the effects of vacuum fluctuations near a photonic band edge. [S1050-2947(98)04511-9]

PACS number(s): 42.50.Fx, 42.50.Lc, 42.70.Qs

I. INTRODUCTION

In recent years, photonic band-gap (PBG) structures have been shown to lead to the localization of light [1] through the carefully engineered interplay between microscopic scattering resonances and the coherent interference of light from many such scatterers [2]. Since the initial proposal of photonic band gaps [3,4], PBG materials exhibiting photon localization have been fabricated at microwave frequencies [5] and more recently, large-scale two-dimensional PBG systems have been produced in the near-infrared [6]. The ultimate goal for laser applications is a full three-dimensional PBG at optical frequencies [7–10]. A PBG comprises a range of frequencies over which linear photon propagation is prohibited. Therefore, atoms with transition frequencies within the gap do not experience the usual fluctuations in the electromagnetic vacuum that are responsible for spontaneous decay. Instead, a photon-atom bound state is formed [11]. Unlike the suppression of spontaneous emission from an atom in a high-Q optical microcavity [12], the bound photon may tunnel many optical wavelengths away from the atom before being reabsorbed. Near a photonic band edge, the photon density of states is rapidly varying, making it dramatically different from the ω^2 dependence found in free space. This implies that the nature of vacuum fluctuations and thus of spontaneous emission near a band edge is radically different from the exponential decay found in free space [13]. More fundamentally, the correlation time of the electromagnetic vacuum fluctuations near a band edge is not negligibly small on the time scale of the evolution of an atomic system coupled to the electromagnetic field. In fact, the reservoir exhibits long-range temporal correlations, making the temporal distinction between atomic system and electromagnetic reservoir unclear. This renders the usual Born-Markov approximation scheme invalid for band edge systems. Studies of single atom spontaneous emission near a photonic band edge [14,15] have shown that this non-Markovian system reservoir interaction gives rise to phenomena such as oscillatory behavior and a fractional steady state population for a single excited atomic state, as well as vacuum Rabi splitting and a subnatural linewidth for atomic emission.

We consider the Dicke model [16,17] for the collective emission of light, or superradiance, from N identical two-level atoms with a transition frequency near a photonic band edge. The study of superradiant emission is of interest not only in its own right, but also because it provides a valuable paradigm for understanding the self-organization and emission properties of a band-edge laser. Of late, there has been a resurgence of interest in superradiance in the context of superradiant lasing action [18], and due to the experimental realization of a true Dicke superradiant system using laser-cooled atoms [19]. A low threshold microlaser operating near a photonic band edge may exhibit unusual dynamical, spectral, and statistical properties. We will show that such effects are already evident in band-edge collective spontaneous emission. A preliminary study of band-edge superradiance for atoms resonant with the band edge [20] has shown that for an atomic system prepared initially with a small collective atomic polarization, a fraction of the superradiant emission remains in the vicinity of the atoms, and a macroscopic polarization emerges in the collective atomic steady state. In addition to this form of spontaneous symmetry breaking, it has been demonstrated that superradiant emission can proceed more quickly and with greater intensity near a photonic band edge than in free space. In the absence of an initial atomic polarization, the early stages of superradiance are governed by fluctuations in the electromagnetic vacuum near the band edge. These fluctuations affect the dynamics of collective decay and will determine the quantum limit of the linewidth of a laser operating near a photonic band edge.

The organization of the paper is as follows. In Sec. II, we present the quantum Langevin equations for collective atomic dynamics in band-edge superradiance. In Sec. III, we calculate an approximate, analytic solution for the equations that describe the N-atom system with low initial inversion of the atomic population. We show that the atoms can exhibit novel emission spectra and a suppression of population fluctuations near a band edge. Sections IV and V treat the case of high initial inversion. In Sec. IV, the mean-field results of Ref. [20] are extended to the case of atoms with resonant frequencies displaced from the band edge. It is shown that the phase and amplitude of the collective atomic polarization can be controlled by an external field that Stark shifts the atomic transition relative to the band edge. The dissipative effect of dipole dephasing is also included in the framework of our non-Markovian system. Section V describes superradiant emission under the influence of vacuum fluctuations by exploiting the temporal division of superradiance into quantum and semiclassical regimes. We find that the system exhibits a macroscopic steady-state polarization amplitude with a phase precession triggered by band-edge quantum fluctuations. In Sec. VI, we describe a method for generating a classical stochastic function that simulates the effect of band-edge vacuum fluctuations. We show that, for a sufficiently large number of atoms, this classical noise ansatz agrees well with the more exact simulations of Sec. V, and may thus be useful in the analysis of band-edge atom-field dynamics. In Appendix A, we give the details of the calculation of the electromagnetic reservoir's temporal autocorrelation function for different models of the photonic band edge. This correlation function is central to determining the nature of atomic decay.

II. EQUATIONS OF MOTION

We consider a model consisting of N two-level atoms with a transition frequency near the band edge coupled to the multimode radiation field in a PBG material. For simplicity, we assume a point interaction, that is, the spatial extent of the active region of the PBG material is less than the wavelength of the emitted radiation. This is often referred to as the small sample limit of superradiance [17]. We neglect the spatially random resonance dipole-dipole interaction (RDDI) near the band edge, which may have a more important impact on atomic dynamics when the atomic transition lies deep within the PBG [20,21]. Nevertheless, our simplified model should provide a good qualitative picture of band-edge collective emission. For an excited atomic state $|2\rangle$ and ground state $|1\rangle$, the interaction Hamiltonian for our system can be written as

$$\mathcal{H} = \sum_\lambda \hbar \Delta_\lambda a_\lambda^\dagger a_\lambda + i\hbar \sum_\lambda g_\lambda (a_\lambda^\dagger J_{12} - J_{21} a_\lambda), \quad (2.1)$$

where a_λ and $a_\lambda^\dagger$ are the radiation field annihilation and creation operators, respectively; $\Delta_\lambda = \omega_\lambda - \omega_{21}$ is the detuning of the radiation mode frequency ω_λ from the atomic transition frequency ω_{21}. $g_\lambda = (\omega_{21} d_{21}/\hbar)(\hbar/2\epsilon_0 \omega_\lambda V)^{1/2} \mathbf{e}_\lambda \cdot \mathbf{u}_d$ is the atom-field coupling constant, where $d_{21}\mathbf{u}_d$ is the atomic dipole moment vector, V is the sample volume, and $\mathbf{e}_\lambda = e_{\mathbf{k},\sigma}$, $\sigma = 1,2$ are the two transverse polarization vectors.

The J_{ij} are collective atomic operators, defined by the relation $J_{ij} \equiv \Sigma_{k=1}^{N} |i\rangle_{kk}\langle j|$; $i,j = 1,2$, where $|i\rangle_k$ denotes the ith level of the kth atom. Using the Hamiltonian (2.1), we may write the Heisenberg equations of motion for the operators of the field modes, $a_\lambda(t)$, the atomic inversion, $J_3(t) \equiv J_{22}(t) - J_{11}(t)$, and the atomic system's collective polarization, $J_{12}(t)$:

$$\frac{d}{dt} a_\lambda(t) = -i\Delta_\lambda a_\lambda(t) + g_\lambda J_{12}(t), \quad (2.2)$$

$$\frac{d}{dt} J_3(t) = -2 \sum_\lambda g_\lambda J_{21}(t) a_\lambda(t) + \text{H.c.}, \quad (2.3)$$

$$\frac{d}{dt} J_{12}(t) = \sum_\lambda g_\lambda J_3(t) a_\lambda(t). \quad (2.4)$$

We may adiabatically eliminate the field operators by formally integrating Eq. (2.2) and substituting the result into Eqs. (2.3) and (2.4). The equations of motion for the collective atomic operators are then

$$\frac{d}{dt} J_3(t) = -2 \int_0^t J_{21}(t) J_{12}(t') G(t-t') dt'$$
$$- 2J_{21}(t)\eta(t) + \text{H.c.}, \quad (2.5)$$

$$\frac{d}{dt} J_{12}(t) = \int_0^t J_3(t) J_{12}(t') G(t-t') dt' + J_3(t)\eta(t). \quad (2.6)$$

Here, $\eta(t) = \Sigma_\lambda g_\lambda a_\lambda(0) e^{-i\Delta_\lambda t}$ is a quantum noise operator that contains the influence of vacuum fluctuations. $G(t-t')$ is the time-delay Green function, or memory kernel, describing the electromagnetic reservoir's average effect on the time evolution of the system operators. The Green function is given by the temporal autocorrelation of the reservoir noise operator,

$$G(t-t') \equiv \langle \eta(t)\eta^\dagger(t') \rangle = \sum_\lambda g_\lambda^2 e^{-i\Delta_\lambda(t-t')}. \quad (2.7)$$

We have made use of the fact that $\langle a_\lambda^\dagger(0) a_\lambda(0) \rangle \simeq 0$, as we are dealing with atomic transition frequencies in the optical domain [13]. In essence, $G(t-t')$ is a measure of the reservoir's memory of its previous state on the time scale for the evolution of the atomic system. In free space, the density of field modes as a function of frequency is broad and slowly varying, resulting in a Green function that exhibits Markovian behavior, $G(t-t') = (\gamma/2)\delta(t-t')$, where γ is the usual decay rate for spontaneous emission [13]. Near a photonic band edge, the density of electromagnetic modes varies rapidly with frequency in a manner determined by the photon dispersion relation, $\omega_{\mathbf{k}}$. We show that this results in long-range temporal correlations in the reservoir that affect the nature of the atom-field interaction.

In order to evaluate $G(t-t')$ near a band edge, we first make the continuum approximation for the field mode sum in Eq. (2.7):

$$G(t-t')=\frac{\omega_{21}^2 d_{21}^2}{2\hbar\,\epsilon_0(2\pi)^3}\int\frac{d^3\mathbf{k}}{\omega_{\mathbf{k}}}e^{-i(\omega_{\mathbf{k}}-\omega_{21})(t-t')}.$$
(2.8)

In this paper, we use an effective-mass approximation to the full dispersion relation for a photonic crystal. Within this approximation, we consider two models for the near-band-edge dispersion. The details of the calculation of $G(t-t')$ for each model and a discussion of its applicability is given in Appendix A. In an anisotropic dispersion model, appropriate to fabricated PBG materials, we associate the band edge with a specific point in k space, $\mathbf{k}=\mathbf{k}_0$. By preserving the vector character of the dispersion expanded about $\mathbf{k}_0$, we account for the fact that, as $\mathbf{k}$ moves away from $\mathbf{k}_0$, both the direction and magnitude of the band-edge wave vector are modified. This gives a dispersion relation of the form

$$\omega_{\mathbf{k}}=\omega_c\pm A(\mathbf{k}-\mathbf{k}_0)^2.$$
(2.9)

Here, $A=2c^2/\omega_{\text{gap}}$, where ω_{gap} is the frequency width of the gap. The positive (negative) sign indicates that $\omega_{\mathbf{k}}$ is expanded about the upper (lower) edge of the PBG, and ω_c is the frequency of the corresponding band edge. This form of dispersion is valid for a gap width $\omega_{\text{gap}}\gg c|\mathbf{k}-\mathbf{k}_0|$, meaning that the effective-mass relation is most directly applicable to large photonic gaps and for wave vectors near the band edge. Furthermore, for a large gap and a collection of atoms that are nearly resonant with the upper band edge, it is a very good approximation to completely neglect the effects of the lower photon bands. The band-edge density of states corresponding to Eq. (2.9) takes the form $\rho(\omega)\sim(\omega-\omega_c)^{1/2}$, $\omega>\omega_c$, characteristic of a three-dimensional phase space. The resulting Green function for $\omega_c(t-t')\gg1$ is

$$G_A(t-t')=\frac{\beta_3^{1/2}e^{i[\pi/4+\delta_c(t-t')]}}{(t-t')^{3/2}},$$

$$t>t'\quad\text{(anisotropic gap)}.$$
(2.10)

In addition to the anisotropic photon dispersion model, it is instructive to consider a simpler isotropic model. In this model, we extrapolate the dispersion relation for a one-dimensional gap to all three spatial dimensions. We thus assume that the Bragg condition is satisfied for the same wave vector magnitude for all directions in k space. This yields an effective-mass dispersion of the form $\omega_k=\omega_c+A(|\mathbf{k}|-|\mathbf{k}_0|)^2$, which associates the band-edge wave vector with a sphere in k space, $|\mathbf{k}|=k_0$. Strictly speaking, an isotropic PBG at finite wave vector $|\mathbf{k}_0|$ does not occur in artificially created, face centered cubic photonic crystals. However, a nearly isotropic gap near $k_0=0$ occurs in certain polar crystals with polaritonic excitations [22]. A simple example of such a crystal is table salt (NaCl), which has a polariton gap in the infrared frequency regime. The band-edge density of states in the isotropic model has the form $\rho(\omega)\sim(\omega-\omega_c)^{-1/2}$, $\omega>\omega_c$, the square-root singularity being characteristic of a one-dimensional phase space. For the Green function we obtain (see Appendix A)

$$G_I(t-t')=\frac{\beta_1^{3/2}e^{-i[\pi/4-\delta_c(t-t')]}}{(t-t')^{1/2}},\quad t>t'\quad\text{(isotropic gap)}.$$
(2.11)

In both Eqs. (2.10) and (2.11), $\delta_c=\omega_{21}-\omega_c$ is the detuning of the atomic resonance frequency from the band edge, and β_α is a constant that depends on the dimension of the band-edge singularity. In particular, for the isotropic model, $\beta_1^{3/2}=\omega_{21}^{7/2}d_{21}^2/12\hbar\,\epsilon_0\pi^{3/2}c^3$, while in the anisotropic model, $\beta_3^{1/2}=\omega_{21}^2 d_{21}^2/8\hbar\,\epsilon_0\omega_c(A\pi)^{3/2}$.

III. LOW ATOMIC EXCITATION: HARMONIC-OSCILLATOR MODEL

In order to understand the effects of band-edge vacuum fluctuations, we begin by presenting a simplified model that permits an analytic solution, and is applicable to a system in which only a small fraction of the two-level atoms are initially in their excited state. This discussion demonstrates how light emission near a photonic band edge can give rise to atomic dynamics, emission spectra, and photon-number statistics that are very different from those expected in free space. We write the atomic operators in the Schwinger boson representation [23]:

$$J_{12}(t)\to b_1^\dagger(t)b_2(t),$$
(3.1)

$$J_3(t)\to b_2^\dagger(t)b_2(t)-b_1^\dagger(t)b_1(t),$$
(3.2)

subject to the constraint on the total number of atoms, $b_1^\dagger(t)b_1(t)+b_2^\dagger(t)b_2(t)=N$. The operators $b_i^\dagger(t)$ and $b_i(t)$ then describe transitions of the system between the excited state $(i=2)$ and the ground state $(i=1)$. In the limit of low atomic excitation, the state $|1\rangle$ has a large population at all times, meaning that we can replace the inversion operator by the classical value $J_3(t)\approx-N$, and that $b_1(t)$ can be approximated by $b_1(t)\approx\sqrt{N}$. In this case, the initially excited two-level atoms behave like a simple harmonic oscillator coupled to the non-Markovian electromagnetic reservoir. In our model, the Heisenberg equations of motion (2.5) and (2.6), reduce to

$$\frac{d}{dt}b_2(t)=-N\int_0^t b_2(t')G(t-t')dt'-\sqrt{N}\,\eta(t).$$
(3.3)

Using the method of Laplace transforms, we can solve for $b_2(t)$ and find

$$b_2(t)=B(t)b_2(0)-\sqrt{N}\sum_\lambda A_\lambda(t)a_\lambda(0),$$
(3.4)

where

$$B(t)=\mathcal{L}^{-1}\{\tilde{B}(s)\},$$
(3.5)

$$\tilde{B}(s)=[s+N\tilde{G}(s)]^{-1},$$
(3.6)

and

$$A_\lambda(t)=\mathcal{L}^{-1}\left\{\frac{g_\lambda}{s+i\Delta_\lambda}\tilde{B}(s)\right\}.$$
(3.7)

$\mathcal{L}^{-1}$ denotes the inverse Laplace transformation, and $\tilde{G}(s)$ is the Laplace transform of the general memory kernel, $G(t-t')$. In this section, we consider the case of an isotropic band edge in the effective-mass approximation [Eq. (2.11)], for which $\tilde{G}(s)$ is written as
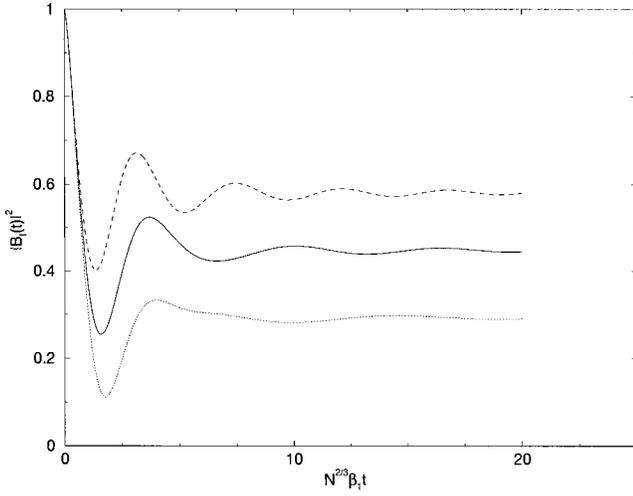
FIG. 1. Normalized population of the excited atomic state near an isotropic photonic band edge for low initial atomic excitation. Various values of the detuning, $\delta_c \equiv \omega_{21} - \omega_c$, of the atomic resonant frequency ω_{21} from a band edge at frequency ω_c are shown. Dashed line, $\delta_c = -0.5$; solid line, $\delta_c = 0$; dotted line, $\delta_c = 0.5$. δ_c is measured in units of $N^{2/3}\beta_1$.

$$\tilde{G}_I(s) = \frac{\beta_1^{3/2} e^{-i\pi/4}}{\sqrt{s - i\delta_c}}. \tag{3.8}$$

For this isotropic Green function, we denote the inverse Laplace transform of Eq. (3.5) by $B_I(t)$. $B_I(t)$ was computed in Ref. [15] in the context of single atom spontaneous emission, and a detailed mathematical derivation may be found therein. Here, it describes the mean or drift evolution of our Heisenberg operator $b_2(t)$. The solution has the form

$$B_I(t) = 2a_1 x_1 e^{N^{2/3}\beta_1 x_1^2 t + i\delta_c t} + a_2(x_2 + y_2)e^{N^{2/3}\beta_1 x_2^2 t + i\delta_c t}$$
$$- \sum_{j=1}^{3} a_j y_j [1 - \Phi(\sqrt{N^{2/3}\beta_1 x_j^2 t})]e^{N^{2/3}\beta_1 x_j^2 t + i\delta_c t}, \tag{3.9}$$

where

$$x_1 = (A_+ + A_-)e^{i\pi/4}, \tag{3.10}$$

$$x_2 = (A_+ e^{-i\pi/6} - A_- e^{i\pi/6})e^{-i\pi/4}, \tag{3.11}$$

$$x_3 = (A_+ e^{i\pi/6} - A_- e^{-i\pi/6})e^{i3\pi/4}, \tag{3.12}$$

$$A_{\pm} = \left\{ \frac{1}{2} \pm \frac{1}{2}\left[1 + \frac{4}{27}\frac{\delta_c^3}{\beta_1^3} \right]^{1/2} \right\}^{1/3}, \tag{3.13}$$

$$y_j = \sqrt{x_j^2}, \quad j = 1,2,3. \tag{3.14}$$

The error function $\Phi(x) = (2/\sqrt{\pi})\int_0^x e^{-t^2}dt$.

The probability of finding the atoms in the excited state is given by $\langle b_2^\dagger(t)b_2(t)\rangle = |B_I(t)|^2$, and is plotted in Fig. 1. We find that the excited-state population exhibits decay and oscillatory behavior before reaching a nonzero steady-state value due to photon localization. These effects are due to the strong dressing of the atoms by the radiation field near a
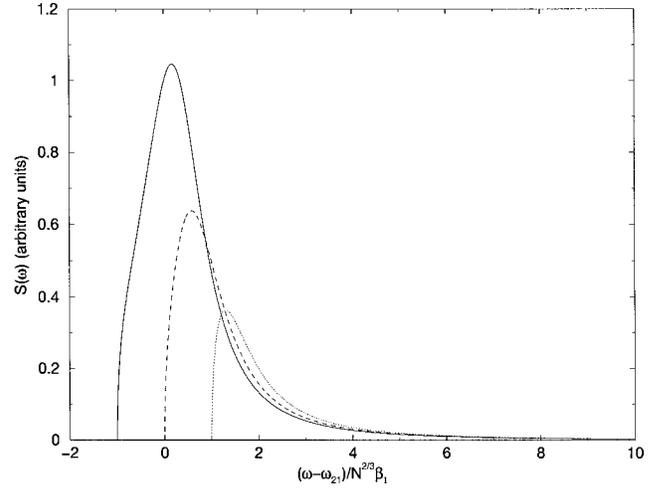

FIG. 2. Collective atomic emission spectrum $\mathcal{S}(\omega)$ (arbitrary units) near an isotropic band edge for low initial atomic excitation. Various values of the detuning, $\delta_c \equiv \omega_{21} - \omega_c$, of the atomic resonant frequency ω_{21} from an isotropic photonic band edge at frequency ω_c are shown. Dotted line, $\delta_c = -1$; dashed line, $\delta_c = 0$; solid line, $\delta_c = 1$. δ_c is measured in units of $N^{2/3}\beta_1$.

photonic band edge, resulting in dressed atomic states that straddle the band edge. Light emission from the dressed state outside the gap results in highly non-Markovian decay of the atomic population, while the dressed state shifted into the gap is responsible for the fractional steady-state population of the excited state. The consequences of this strong atom-field interaction are discussed in detail for single-atom spontaneous emission in Ref. [15], and for superradiant emission in Secs. IV and V of this paper. We note that the degree of steady-state localization is a sensitive function of the detuning, δ_c, of the atomic resonance from the band edge. The decay rate scales as $N^{2/3}\beta_1 t$ for the isotropic model. However, there is no evidence for the buildup of interatomic coherence, as very few of the atoms are initially excited.

Equation (3.4) also allows us to calculate the system's emission spectrum into the modes ω for an atom with resonant frequency ω_{21} using the relation

$$\mathcal{S}(\omega) = \int_0^\infty e^{-i(\omega - \omega_{21})\tau}\langle b_2^\dagger(\tau)b_2(0)\rangle d\tau + \text{c.c.}$$

$$\sim \text{Re}\{\tilde{B}^*[i(\omega - \omega_{21})]\}, \tag{3.15}$$

where $\tilde{B}(s)$ is defined in Eq. (3.6). The spectrum for the isotropic model is then

$$\mathcal{S}_I(\omega) \simeq \begin{cases} 0, & \omega \leq \omega_c \\ N\beta_1^{3/2}\dfrac{\sqrt{\omega - \omega_c}}{N^2\beta_1^3 + (\omega - \omega_{21})^2(\omega - \omega_c)}, & \omega > \omega_c. \end{cases} \tag{3.16}$$

This spectrum is shown in Fig. 2, and differs significantly from the Lorentzian spectrum for light emission in free space. In fact, the emission spectrum is not centered about the atomic resonant frequency, which is what one would expect for an atom decaying to an unrestricted vacuum mode density. We see that for an arbitrary detuning, δ_c, of ω_{21}

from the band edge, the emission spectrum vanishes for frequencies at the band edge and within the gap, $\omega \lesssim \omega_c$. This is consistent with the localization of light near the atoms for electromagnetic modes within the PBG. As ω_{21} is detuned further into the gap, spectral results confirm that a greater fraction of the light is localized in the gap dressed state, as the total emission intensity out of the decaying dressed state is reduced. Conversely, as ω_{21} is moved out of the gap, the emission profile becomes closer to a Lorentzian in form and the total emitted intensity increases. The spectral linewidth ratio between the isotropic band edge and free space is of the order of $\beta_1/(\gamma N^{1/3})$, while for an anisotropic band edge it is $\sim N \beta_3/\gamma$. This corresponds to the fact that collective emission is much more rapid near an anisotropic band edge than in free space, whereas it is slower than in free space for the isotropic model.

It is also instructive to evaluate the quantum fluctuations in the atomic inversion in the context of the harmonic-oscillator model. Variances in the atomic population can be written in terms of the Mandel Q parameter [24],

$$Q(t) = \frac{\langle n^2(t) \rangle - \langle n(t) \rangle^2}{\langle n(t) \rangle}, \quad (3.17)$$

where $n(t) \equiv b_2^\dagger(t) b_2(t)$ is the number operator for the occupation of the excited state. Since both the free space and PBG solutions in our model can be written in the form of Eq. (3.4), we can write the Q parameter in the general form

$$Q(t) = |B(t)|^2 Q(0) + N \sum_\lambda |A_\lambda(t)|^2. \quad (3.18)$$

Again, $|B(t)|^2$ is the normalized probability of finding the initially excited fraction of the atoms still in the excited state at time t. For an isotropic band edge, $B(t) = B_I(t)$ [Eq. (3.9)], whereas in free space, $B(t) \sim e^{-N\gamma t/2}$, representing the exponential decay of the excited-state population. Using the identity $N \sum_\lambda |A_\lambda(t)|^2 = 1 - |B(t)|^2$, as derived in Appendix B, we can write the population fluctuations as

$$Q(t) = |B(t)|^2 [Q(0) - 1] + 1. \quad (3.19)$$

For arbitrary initial statistics, atoms in free space decay to the vacuum state with $Q(t) = 1$; since the atoms decay fully, there are no meaningful atomic statistics in the long-time limit. $Q(t)$ is plotted in Fig. 3 for the isotropic band edge ($\delta_c = 0$) for the cases $Q(0) = 0$, 1, and 2. Near the band edge, photon localization prevents the atomic system from decaying to the ground state. We find instead that the steady-state statistics are sensitive to the statistics of the initial state and to the value of δ_c. A system initially prepared with super-Poissonian statistics [$Q(0) > 1$] experiences a *suppression* of population fluctuations in the steady state. In a system that is initially sub-Poissonian [$Q(0) < 1$], the fluctuations increase, but are held below the Poissonian level by photon localization. In both cases, the steady-state value of the atomic population fluctuations is controlled by δ_c. Our harmonic oscillator model thus suggests that a PBG system may exhibit atypical quantum statistics in the absence of a cavity or external fields. It is important to extend the analysis of collective emission under the influence of vacuum fluctua-
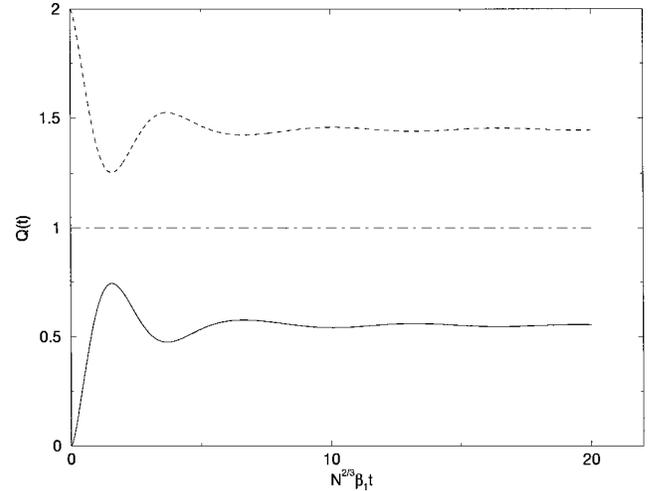

FIG. 3. Fluctuations in the excited-state atomic population as measured by the Mandel parameter, $Q(t) = [\langle n^2(t) \rangle - \langle n(t) \rangle^2]/\langle n(t) \rangle$, for low initial excitation for an atomic resonant frequency tuned to an isotropic photonic band edge, $\delta_c = 0$. Dashed line, $Q(0) = 2$; solid line, $Q(0) = 0$. Double-dashed line denotes fluctuations for Poissonian population variance, $Q(0) = 1$.

tions to the high excitation (superradiant) regime. In this case, the two-level nature of the atomic operators will become important and will modify the quantum statistics from that of the harmonic-oscillator picture. This generalization is considered in the next two sections.

IV. HIGH ATOMIC EXCITATION: MEAN-FIELD SOLUTION

When the atomic system is initially fully or nearly fully inverted, we expect interatomic coherences, transmitted via the atomic polarizations, to have a strong influence on emission dynamics. For such high initial atomic excitation, the quantum Langevin equations (2.5) and (2.6), paired with the non-Markovian memory kernels (2.10) or (2.11), do not possess an obvious analytic solution. Moreover, conventional perturbation theory applied to these equations fails to recapture the influence of the photon-atom bound state [11], which plays a crucial role in band-edge radiation dynamics. However, when the superradiant system is prepared with a non-zero initial polarization [$J_{12}(0) \neq 0$], the average dipole moment dominates the incoherent effect of the vacuum fluctuations and the subsequent evolution is well described by a semiclassical approximation [17]. In this case, it is possible to factorize the atomic operator equations:

$$\frac{d}{dt}\langle J_3(t) \rangle = -4 \, \mathrm{Re}\left\{ \langle J_{21}(t) \rangle \int_0^t \langle J_{12}(t') \rangle G(t-t') dt' \right\}, \quad (4.1)$$

$$\frac{d}{dt}\langle J_{12}(t) \rangle = \langle J_3(t) \rangle \int_0^t \langle J_{12}(t') \rangle G(t-t') dt'. \quad (4.2)$$

The brackets $\langle \mathcal{O} \rangle$ denote the quantum-mechanical average of the Heisenberg operator $\mathcal{O}$ over the Heisenberg picture atom-field state vector, $|\Psi\rangle = |\mathrm{vac}\rangle \otimes |\psi\rangle$, where $|\mathrm{vac}\rangle$ represents the electromagnetic vacuum state, and $|\psi\rangle$ represents the ini-
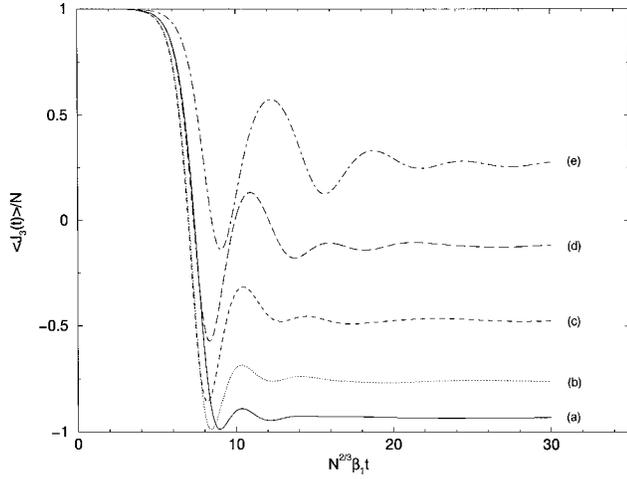
FIG. 4. Mean-field solution for the atomic inversion, $\langle J_3(t)\rangle/N$, near an isotropic photonic band edge, starting with an infinitesimal initial polarization, $r=10^{-5}$. Various values of the detuning, $\delta_c \equiv \omega_{21}-\omega_c$, of the atomic resonant frequency ω_{21} from a band edge at frequency ω_c are shown. (a) $\delta_c=1$; (b) $\delta_c=0.5$; (c) $\delta_c=0$; (d) $\delta_c=-0.5$; (e) $\delta_c=-1$. δ_c is measured in units of $N^{2/3}\beta_1$.

tial state of the atomic system. Clearly in this mean-field approach, the quantum noise contribution is neglected, as $\langle\eta(t)\rangle=0$. Recently, Bay, Lambropoulos, and Mølmer [25] found that, for a simpler Fano profile gap model, the dynamics of superradiant emission are affected by the choice of factorization applied to the full quantum equations. However, the complete factorization used here retains the qualitative features and evolution time scales of more elaborate factorization schemes. Equations (4.1) and (4.2) were solved numerically in Ref. [20] for an atomic resonance frequency coincident with the band edge ($\delta_c=0$) and a small initial collective polarization. The initial collective state was assumed to be of the form

$$|\psi\rangle = \prod_{k=1}^{N} (\sqrt{r}|1\rangle + \sqrt{1-r}|2\rangle)_k \qquad (4.3)$$

with $r\ll1$, so that initially the atoms are almost fully inverted. In this paper, we extend the previous analysis to atomic frequencies detuned from the band edge. Despite its neglect of vacuum fluctuations, mean-field theory illuminates many of the interesting features of the system. The relationship between mean-field theory and a more complete description including quantum fluctuations is discussed in Sec. V.

For clarity, we discuss separately the atomic dynamics in our isotropic and anisotropic dispersion models. Figures 4 and 5 show the inversion per atom and the average polarization amplitude per atom respectively for various values of δ_c near an isotropic band edge. We see from Fig. 4 that a fraction of the superradiant emission remains localized in the vicinity of the atoms in the steady state, due to the Bragg reflection of collective radiative emission back to the atoms. This localized light exhibits a nonzero expectation value for the field operator, which in turn leads to the emergence of a macroscopic polarization amplitude in the steady state. We further note that the decay rate for the upper atomic state is proportional to $N^{2/3}$. Accordingly, the peak radiation inten-
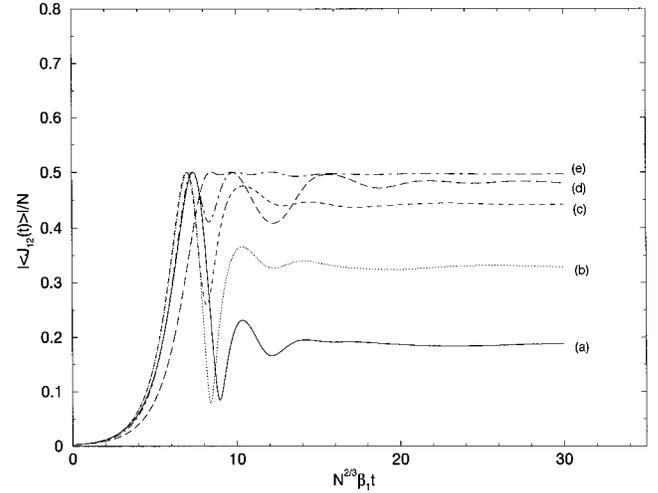

FIG. 5. Mean-field solution for the atomic polarization amplitude, $|\langle J_{12}(t)\rangle|/N$, near an isotropic photonic band edge, starting with an infinitesimal initial polarization, $r=10^{-5}$. Various values of the detuning, $\delta_c \equiv \omega_{21}-\omega_c$, of the atomic resonant frequency ω_{21} from a band edge at frequency ω_c are shown. (a) $\delta_c=1$; (b) $\delta_c=0.5$; (c) $\delta_c=0$; (d) $\delta_c=-0.5$; (e) $\delta_c=-1$. δ_c is measured in units of $N^{2/3}\beta_1$.

sity is proportional to $N^{5/3}$. This is to be compared with the values N and N^2 for the free space decay rate and peak radiation intensity, respectively.

As in single-atom spontaneous emission near an isotropic band edge [15], the dressing of the atoms by their own radiation field causes a splitting of the band of collective atomic states such that the collective spectral density vanishes at the band-edge frequency. The strongly dressed atomic states are repelled from the band edge, with some levels being pulled into the gap and the remaining levels being pushed into the electromagnetic continuum outside the PBG. In the long-time (steady-state) limit, the energy contained in the dressed states outside the band gap decays whereas the energy in the states inside the gap remains in the vicinity of the emitting atoms. It is the localized light associated with the gap dressed states that sustains the fractionalized steady-state inversion and nonzero atomic polarization. For the isotropic model, this splitting and fractional localization persist even when ω_{21} lies just outside the gap ($\delta_c>0$), and the fraction of localized light in the steady state increases as ω_{21} moves towards and enters the gap. In the dressed-state picture, the self-induced oscillations in both the inversion and the polarization that occur during radiative emission can be interpreted as being due to interference between the dressed states. The oscillation frequency is proportional to the frequency splitting between the upper and lower collective dressed states. This is the analog of the collective Rabi oscillations of N Rydberg atoms in a resonant high-Q cavity [26]. From Fig. 4, we see that a dressed state outside the band gap decays more slowly for atomic resonant frequencies deeper inside the gap, causing the collective oscillations to persist over longer periods of time. Clearly, this decay is nonexponential and highly non-Markovian in nature. Figure 5 confirms that, as required, the polarization amplitude for large negative values of δ_c is constrained by the condition, $\langle J_{12}(t)\rangle/N\leqslant1/2$.

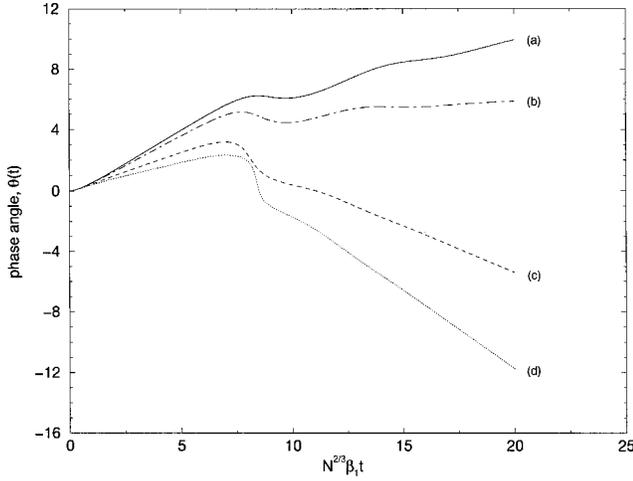In Fig. 6, we plot the phase angle of the collective

FIG. 6. Mean-field solution for the phase angle (in radians) of the atomic polarization, $\theta(t)$, near an isotropic photonic band edge, starting with an infinitesimal initial polarization, $r=10^{-5}$. Various values of the detuning, $\delta_c \equiv \omega_{21} - \omega_c$, of the atomic resonant frequency ω_{21} from a band edge at frequency ω_c are shown. (a) $\delta_c = 0.5$; (b) $\delta_c = 0$; (c) $\delta_c = -0.75$; (d) $\delta_c = -1$. δ_c is measured in units of $N^{2/3}\beta_1$.

atomic polarization in the isotropic model, $\theta(t)$ $= \tan^{-1}\{\mathrm{Im}\langle J_{12}(t)\rangle / \mathrm{Re}\langle J_{12}(t)\rangle\}$. Prior to atomic emission, this phase angle rotates at a constant rate, and in the vicinity of the decay process $\theta(t)$ exhibits the effects of collective Rabi oscillations. When the emission is complete, the rate of change of phase angle, $\dot{\theta}(t)$, attains a new steady-state value, $\dot{\theta}(t_s)$, that depends sensitively on the detuning frequency δ_c. $\dot{\theta}(t_s)$ is a measure of the energy difference between the bare atomic state and the localized dressed state, $\hbar(\omega_{21} - \omega_{\mathrm{loc}})$. Such a polarization phase rotation implies that the collective atomic Bloch vector of the system exhibits precessional dynamics in the steady state. Unlike the conventional precession [27] of atomic dipoles in an ordinary vacuum driven by an external laser field, Bloch vector precession in a PBG occurs in the absence of an external driving field. Instead, the precession is driven by the self-organized state of light generated by superradiance, which remains localized near the emitting atoms. We see in Fig. 6 that for values of δ_c such that $\omega_{21} - \omega_{\mathrm{loc}} < 0$, $\dot{\theta}(t_s)$ is negative, while for $\omega_{21} - \omega_{\mathrm{loc}} > 0$, $\dot{\theta}(t_s)$ is positive, i.e., the phase is rotating in the opposite direction. At a detuning corresponding to a constant phase in the steady state $[\dot{\theta}(t_s) = 0]$, the dressed and bare states are of the same energy; this occurs for a detuning value of $\delta_c = -0.644 N^{2/3}\beta_1$. At this value of δ_c, we also find that $\langle J_3(t_s)\rangle = 0$, implying that there is no net absorption of light by the atomic system. This is, in essence, a collective transparent state [27].

Collective emission dynamics near an anisotropic band edge are pictured in Figs. 7 and 8. For ω_{21} coincident with the band edge or slightly within the gap ($\delta_c \le 0$), we again find a fractional atomic inversion in the steady state (Fig. 7). Rabi oscillations in the atomic population are much less pronounced than in the isotropic model, even for ω_{21} detuned into the gap. This demonstrates that the dressed atomic states outside a physical photonic band gap decay much more rapidly than the isotropic model would suggest. Furthermore,
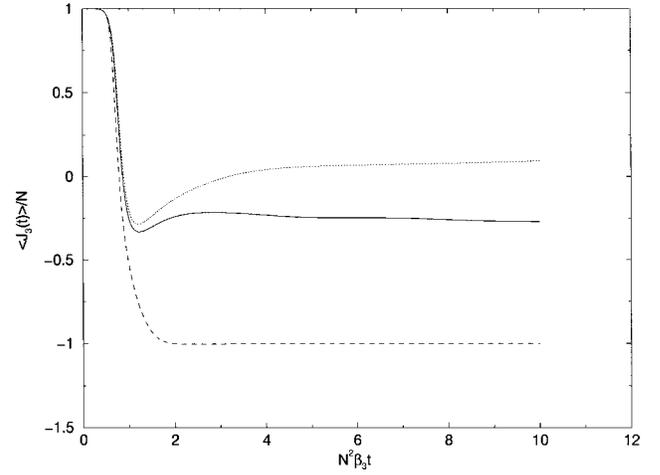

FIG. 7. Mean-field solution for the atomic inversion, $\langle J_3(t)\rangle / N$, near an anisotropic photonic band edge, starting with an infinitesimal initial polarization, $r=10^{-6}$. Various values of the detuning, $\delta_c \equiv \omega_{21} - \omega_c$, of the atomic resonant frequency ω_{21} from a band edge at frequency ω_c are shown. Dashed line, $\delta_c = 0.1$; solid line, $\delta_c = 0$; dotted line, $\delta_c = -0.3$. δ_c is measured in units of $N^2\beta_3$.

in contrast with the isotropic model, we see that photon localization is lost for even a small detuning of ω_{21} into the continuum of field modes outside the band gap. Therefore, while we find a macroscopic steady-state polarization and precessional dynamics of the Bloch vector for $\delta_c \le 0$ (Fig. 8), for $\delta_c > 0$ the polarization dies away after collective emission has taken place. Photon localization from an atomic level lying just outside the gap in a three-dimensional PBG material may, however, be realized through quantum interference effects if there is a third atomic level lying slightly inside the gap [28]. These results point to the greater sensitivity of the atomic dynamics to the more realistic anisotropic band edge. Because the isotropic model overestimates the momentum space for photons satisfying the Bragg condition, photon lo-
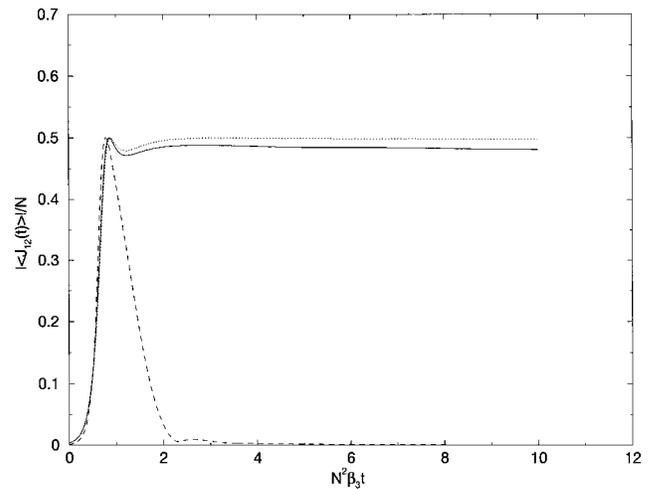

FIG. 8. Mean-field solution for the atomic polarization amplitude, $|\langle J_{12}(t)\rangle| / N$, near an anisotropic photonic band edge, starting with an infinitesimal initial polarization, $r=10^{-6}$. Various values of the detuning, $\delta_c \equiv \omega_{21} - \omega_c$, of the atomic resonant frequency ω_{21} from a band edge at frequency ω_c are shown. Dashed line, $\delta_c = 0.1$; solid line, $\delta_c = 0$; dotted line, $\delta_c = -0.3$. δ_c is measured in units of $N^2\beta_3$.

calization effects and vacuum Rabi splitting are exaggerated in the isotropic model relative to an engineered photonic crystal. In the anisotropic model, the phase space available for propagation vanishes as the optical frequency approaches the band edge. As a result, vacuum Rabi splitting pushes the collective atomic dressed state into a region with a larger density of electromagnetic modes. Consequently, the decay rate of the atomic inversion is proportional to N^2 near the anisotropic band edge, and the corresponding peak radiation intensity is proportional to N^3. Clearly, superradiance near an anisotropic PBG can proceed more quickly and can be more intense than in free space. As a result, PBG superradiance may enable the design of mirrorless, low-threshold microlasers exhibiting ultrafast modulation speeds.

From polarization phase and amplitude results, we conclude that (i) unlike in free space, the atoms near a photonic band edge attain a fractionally inverted state with constant polarization amplitude and rate of change of phase angle. This corresponds to a macroscopic atomic coherence in the steady state analogous to that experienced in a laser. In our case, however, ‘‘lasing’’ occurs in the band-edge continuum rather than into a conventional cavity mode. (ii) By varying the value of δ_c, one may control the direction and rate of change of the steady-state polarization phase angle. This may be realized by applying a small external dc field to the sample that Stark shifts the atomic transition frequency of the atoms. This type of control over the collective atomic Bloch vector may be of importance in the area of information storage and optical memory devices [29,30].

The above analysis makes it clear that collective spontaneous emission dynamics in a PBG are significantly different from those in free space. In a real PBG material, the dephasing of atomic dipoles due to interatomic collisions or phonon-atom interactions may also have a significant effect on the evolution of our system over a large range of temperatures. In the free space Markov approach, dipole dephasing is described by a phenomenological polarization decay constant [31]. Since the Markov approximation does not apply near a band edge, one cannot account for dephasing by simply adding a phenomenological decay term to Eq. (4.2). However, we expect that the atomic resonant frequency will experience random Stark shifts due to atom-atom or atom-phonon interactions. This effect can be included in the description of our system by adding a variation Δ to the detuning frequency δ_c at each time step in a computational simulation of Eqs. (4.1) and (4.2). Δ is chosen to be a Gaussian random number with zero mean. The width of the Gaussian distribution is determined by the magnitude of the random Stark effect. Such a simulation in free space would include a random Δ only in the equation for the atomic polarization. This is because the slowly varying photon density of states seen by the atoms at the frequency $\omega_{21} + \Delta$ does not change significantly with typical homogeneous line broadening effects. In contrast, we have seen that near a photonic band edge, slight variations in δ_c may drastically change the atomic inversion. Therefore we include Δ in both system equations. In Fig. 9, we plot the evolution of the collective inversion and polarization under the simulated collision broadening described above. The random Stark shifts lead to the loss of macroscopic polarization and the loss of atomic inversion in the long-time limit. The latter effect can be understood by noting that the random frequency shifts are sym-
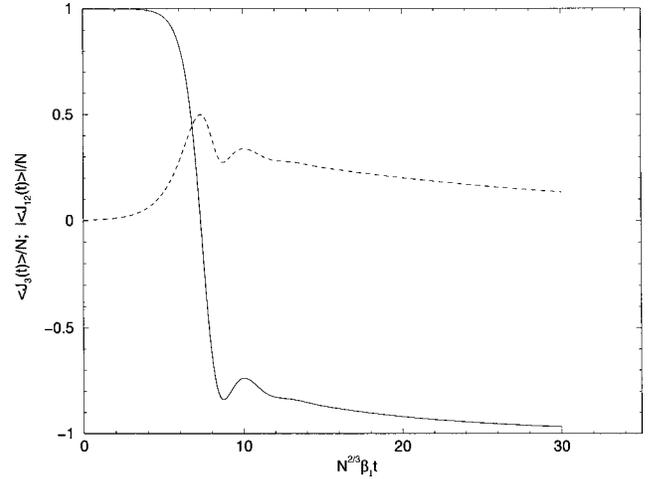

FIG. 9. Mean-field solution for the atomic inversion (solid line) and polarization amplitude (dashed line) under the influence of collision broadening for an atomic resonant frequency at an isotropic photonic band edge, $\delta_c = 0$. The system is given an infinitesimal initial polarization, $r = 10^{-5}$. The simulated Stark shift is a Gaussian random distribution with zero mean and standard deviation $0.5 N^{2/3} \beta_1$.

metrically distributed about the mean resonant frequency. Frequency shifts into the gap promote photon localization, while those away from the gap cause further decay of the atomic inversion. Over time, the net result is that the frequency shifts away from the gap encourage the decay of the atomic population. This is true even in atomic systems for which the mean resonant frequency lies within the gap. From the above considerations, it is clear that dephasing is a significant perturbation on photon localization near a photonic band edge. As in the case of a conventional laser, the effects of dephasing may be partially compensated for by external pumping.

Although a superradiant system can be prepared in a coherent initial state of the type described by Eq. (4.3) [27], collective emission is typically initiated by spontaneous emission, a random, incoherent process. Over time, spontaneous emission leads to the buildup of macroscopic coherence in the sample. The effect of vacuum fluctuations is then of considerable importance in the full description of superradiance, both from a fundamental point of view, and for potential device applications, such as the recently proposed superradiant laser [18]. In the next section, we present a more detailed description of PBG superradiance that takes into account the role of quantum fluctuations.

V. BAND-EDGE SUPERRADIANCE AND QUANTUM FLUCTUATIONS

In order to describe the evolution of the superradiant system's collective Bloch vector under the influence of quantum fluctuations, we consider atomic operator correlation functions of the form [32]

$$g^{pq} = \langle (J_{12})^p (J_{21})^q \rangle. \tag{5.1}$$

Here the operators are evaluated at equal times. As in free space, we expect vacuum fluctuations to drive the system

from its unstable initial state with all atoms inverted to a new stable equilibrium state. Such fluctuations are particularly relevant prior to the buildup of macroscopic atomic polarization. Indeed, they provide the trigger for superradiant emission. In the early-time, inverted regime, we may set $J_3(t) = J_3(0)$ in Eqs. (2.5) and (2.6), giving

$$\frac{d}{dt} J_{12}(t) = \int_0^t dt' J_3(0) J_{12}(t') G(t-t') + J_3(0) \eta(t).$$

(5.2)

The resulting equation remains nonlinear, and involves products of atomic and reservoir operators. We may simplify expressions containing operators in this inverted regime by considering operator averages over only the atomic Hilbert space. For an arbitrary Heisenberg operator $\mathcal{O}(t)$, we denote the atomic expectation value for an initial fully inverted state $|I\rangle$ by $\langle \mathcal{O} \rangle_A \equiv \langle I | \mathcal{O} | I \rangle$. We denote by the set $\{|\lambda\rangle\}$ a complete set of 2^N normalized basis vectors for the atomic Hilbert space including $|I\rangle$, such that $\langle \lambda | I \rangle = \delta_{\lambda, I}$, where $\delta_{\alpha, \beta}$ is the Kronecker delta function. Clearly, $\langle I | J_3(0) | \lambda \rangle = N \delta_{I, \lambda}$. Since $J_3(0)$ acts as a source term for $J_{12}(t)$ in Eq. (5.2), we also have the property $\langle I | J_{12}(t) | \lambda \rangle = 0$ for $\lambda \neq I$ in the inverted regime. This can be shown by considering the equation of motion for $\langle I | J_{12}(t) | \lambda \rangle$:

$$\frac{d}{dt} \langle I | J_{12}(t) | \lambda \rangle = \int_0^t dt' \sum_\mu \langle I | J_3(0) | \mu \rangle \langle \mu | J_{12}(t') | \lambda \rangle$$

$$\times G(t-t') + \langle I | J_3(0) | \lambda \rangle \eta(t)$$

$$= N \int_0^t dt' \langle I | J_{12}(t') | \lambda \rangle G(t-t') + N \delta_{I, \lambda} \eta(t),$$

(5.3)

where μ labels a complete set of atomic states. This integrodifferential equation satisfies the initial condition $\langle I | J_{12}(0) | \lambda \rangle = 0$, since $J_{12}(0)$ acts as a raising operator on the fully inverted bra vector $\langle I |$. For $\lambda \neq I$, the source term in Eq. (5.3) is also absent, leading to the solution $\langle I | J_{12}(t) | \lambda \rangle = 0$. Using this property, we may replace the atomic average over products of atomic operators with products of atomic averages, provided that $J_3(t) = J_3(0)$. For example,

$$\langle J_{12} J_{21} \rangle = \sum_\mu \langle \text{vac} | \otimes \langle I | J_{12} | \mu \rangle \langle \mu | J_{21} | I \rangle \otimes | \text{vac} \rangle$$

$$= \langle \langle J_{12} \rangle_A \langle J_{21} \rangle_A \rangle_R.$$

(5.4)

Here, $\langle \mathcal{O} \rangle_R \equiv \langle \text{vac} | \mathcal{O} | \text{vac} \rangle$ denotes an expectation value over the reservoir variables. For an arbitrary moment g^{pq}, we have

$$g^{pq} = \langle \langle J_{12} \rangle_A^p \langle J_{21} \rangle_A^q \rangle_R.$$

(5.5)

We note that such a factorization is valid only for an antinormal ordering of the polarization operators, since $\langle I | J_{21}(t) | \lambda \rangle$ does not vanish in general.

Taking the atomic expectation value of Eq. (5.2), we obtain

$$\frac{d}{dt} \langle J_{12}(t) \rangle_A = N \int_0^t \langle J_{12}(t') \rangle_A G(t-t') dt' + N \eta(t).$$

(5.6)

This is a linear equation that has lost its operator character over the atomic variables but not over the electromagnetic reservoir, as evidenced by the presence of the quantum noise operator, $\eta(t)$. Equation (5.6) can be solved by the method of Laplace transforms. The solution has the form

$$\langle J_{12}(t) \rangle_A = D(t) \langle J_{12}(0) \rangle_A + N \sum_\lambda C_\lambda(t) a_\lambda(0), \quad (5.7)$$

where

$$D(t) = \mathcal{L}^{-1} \{ \tilde{D}(s) \}, \tag{5.8}$$

$$\tilde{D}(s) = [s - N\tilde{G}(s)]^{-1}, \tag{5.9}$$

and

$$C_\lambda(t) = \mathcal{L}^{-1} \left\{ \frac{g_\lambda}{s + i\Delta_\lambda} \tilde{D}(s) \right\}. \tag{5.10}$$

Again, $\mathcal{L}^{-1}$ denotes the inverse Laplace transform. The Laplace transformation of the memory kernel for an isotropic band edge, $\tilde{G}_I(s)$, is given in Eq. (3.8). Despite the fact that $\langle J_{12}(0) \rangle_A = 0$, we retain the first term in Eq. (5.7) for later notational convenience.

The early-time quantum fluctuations in a superradiant system prevent us from predicting *a priori* the evolution of any single experimental realization of the atoms. Instead, we can only determine the probability of a particular trajectory of the collective atomic Bloch vector. In order to obtain the statistics of a band-edge superradiant pulse, we first determine the statistics of the collective Bloch vector for a set of identically prepared systems after each has passed through the early-time regime governed by vacuum fluctuations. The relevant time scale will be referred to as the quantum to semiclassical evolution *crossover time*, $t = t_0$. Our approach is to calculate the phase and amplitude distributions of the polarization at the crossover time quantum mechanically. The subsequent ($t > t_0$) evolution of the ensemble is then obtained by solving the semiclassical equations (4.1) and (4.2) using the polarization distribution function at t_0. In other words, the distribution of values of $\langle J_{12}(t_0) \rangle$ obtained from the early-time quantum fluctuations provide the initial conditions for subsequent, semiclassical evolution. In order to implement this approach, we must first identify t_0 for our system [17,33]. One expects such a transition to occur in the high atomic inversion regime, $\langle J_3(t) \rangle \simeq N$. It is natural to define t_0 such that for $t > t_0$ the expectation value of the commutator of the system operators $J_{21}(t)$ and $J_{12}(t)$ becomes very small compared to the expectation value of their product [17]. This gives the condition

$$\langle J_{21}(t) J_{12}(t) \rangle \gg \langle [J_{21}(t), J_{12}(t)] \rangle, \quad t > t_0. \quad (5.11)$$

Evaluating the above commutator, we have $\langle [J_{21}(t), J_{12}(t)] \rangle = \langle J_3(t) \rangle$, which is equal to N for full atomic inversion. From Eqs. (5.5) and (5.7), we find that

$$\langle J_{21}(t)J_{12}(t)\rangle = \langle J_3(t)+J_{12}(t)J_{21}(t)\rangle$$

$$= N\left[1+N\sum_\lambda |C_\lambda(t)|^2\right] = N|D(t)|^2. \tag{5.12}$$

The last equality is obtained by use of the identity $N\Sigma_\lambda |C_\lambda(t)|^2 = |D(t)|^2-1$, as derived in Appendix B. In free space, $|D(t)|^2 = e^{N\gamma t}$, giving the crossover time, $t_0^{\text{free}} \simeq 1/N\gamma$. One can solve for the crossover time near a band edge, t_0^{PBG}, computationally. In the isotropic model, for $\delta_c = 0$ we find that $t_0^{\text{PBG}} \simeq 1.24/N^{2/3}\beta_1$. The crossover time maintains this $1/N^{2/3}\beta_1$ dependence for ω_{21} displaced from the band edge. The corresponding time scale for the anisotropic gap is $1/N^2\beta_3$. The buildup of a macroscopic polarization then occurs more slowly near an isotropic band edge and more quickly near an anisotropic band edge than in free space.

Using a semiclassical approach, we may write the value of the polarization at any time $t \geq t_0$ in terms of an amplitude κ and a phase angle ϕ, $\langle J_{12}(t)\rangle^{\text{Cl}} \equiv J(\kappa,\phi,t)$. The superscript Cl refers to the fact that the expectation value $\langle\;\rangle^{\text{Cl}}$ is taken in the semiclassical regime $t \geq t_0$. We define $P(\kappa)d\kappa$ as the probability of finding the amplitude between κ and $\kappa+d\kappa$, and $Q(\phi)d\phi$ as the probability of finding the phase angle between ϕ and $\phi+d\phi$. We may then write the moments of the macroscopic polarization distribution as

$$\langle (J_{12}(t))^p(J_{21}(t'))^q\rangle^{\text{Cl}} = \int d\kappa \int d\phi P(\kappa)Q(\phi)$$
$$\times [J(\kappa,\phi,t)]^p[J^*(\kappa,\phi,t')]^q. \tag{5.13}$$

For $t=t_0$, we assume that the polarization has the form $J(\kappa,\phi,t)=\kappa e^{i\phi}$, giving for the moments

$$\langle (J_{12}(t_0))^p(J_{21}(t_0))^q\rangle^{\text{Cl}}$$
$$= \int d\kappa \int d\phi P(\kappa)Q(\phi)\kappa^{p+q}e^{i(p-q)\phi}. \tag{5.14}$$

The quantum analog, $\langle\;\rangle^Q$, of Eq. (5.14) can be written in the form of Eq. (5.5) evaluated at $t=t_0$. Substituting Eq. (5.7) and its adjoint into Eq. (5.5) yields

$$\langle (J_{12}(t_0))^p(J_{21}(t_0))^q\rangle^Q$$
$$= N^{p+q}\left\langle \left[\sum_\lambda C_\lambda(t_0)a_\lambda(0)\right]^p\left[\sum_\lambda C_\lambda^*(t_0)a_\lambda^\dagger(0)\right]^q\right\rangle_R. \tag{5.15}$$

As the reservoir expectation value is taken over the the operators a_λ, which satisfy a Gaussian probability distribution, Wick's theorem [13] is applied in order to reduce the operator averages of products of field operators to averages over products of pairs of field operators. We then have

$$\langle (J_{12}(t_0))^p(J_{21}(t_0))^q\rangle^Q \simeq \delta_{pq}N^p p!|D(t_0)|^{2p}. \tag{5.16}$$

This expression has corrections of order N^{p-1}, meaning that it is asymptotically valid for large N. Equating Eqs. (5.14) and (5.16), we solve for the distributions $P(\kappa)$ and $Q(\phi)$ to obtain the desired initial polarization distribution for the semiclassical superradiance equations. The early time distributions for free space and the band edge differ only in the form of the function $D(t)$, as the above analysis makes no other distinction between the two cases. Thus in the band-edge system, as in free space, the entire effect of the early time atomic evolution can be recaptured using the distribution of initial conditions given at $t=t_0$. The phase of the polarization is given by the relation

$$\int_0^{2\pi} d\phi e^{i(p-q)\phi}Q(\phi) = \delta_{p,q}. \tag{5.17}$$

This shows that $Q(\phi)$ is uniformly distributed between 0 and 2π. The initial polarization amplitude distribution is found from the relation

$$\int_0^\infty d\kappa P(\kappa)\kappa^{2p} = p![N|D(t_0)|^2]^p. \tag{5.18}$$

The result is a Gaussian distribution of width $N|D(t_0)|^2$ centered at zero,

$$P(\kappa) = \frac{1}{\sqrt{\pi N|D(t_0)|^2}}\exp\left[\frac{-\kappa^2}{N|D(t_0)|^2}\right]. \tag{5.19}$$

It has been shown via density matrix methods [17] that in free space one may choose the crossover time anywhere in the inverted regime, the simplest choice being $t_0=0$. This is due to the absence of temporal correlations of the reservoir for $t\neq t'$. Figure 10 shows the ensemble-averaged collective emission in free space and at an isotropic band edge ($\delta_c = 0$) for $N=100$ atoms. Both the free space and band edge systems are shown for two choices of initial polarization distribution. The solid lines correspond to the choice of $t_0=0$ in the amplitude distribution (5.19) for both free space and the band edge. The dashed lines correspond to the choice $t_0 = t_0^{\text{free}}$ and $t_0=t_0^{\text{PBG}}$ for the free-space and band-edge systems, respectively. As per Eq. (5.17), the initial phase of the polarization in all cases is chosen from a uniform random distribution. As expected, Fig. 10 demonstrates that the choice of t_0 is unimportant in free space, so long as it is chosen in the inverted regime. Near a photonic band edge, we see that the choice of t_0 affects the later evolution of the system. In particular, it affects the onset time for collective emission. It is clear from these simulations that the details of the non-Markovian evolution in the quantum regime play a crucial role in the subsequent semiclassical evolution of the band edge superradiance. The long-range temporal correlations of the reservoir require that we treat the vacuum fluctuations explicitly throughout the quantum evolution of the system. A similar picture holds in the case of an anisotropic PBG material. In our anisotropic model, memory of the initial state is expressed through the Green function (2.10). In this case, superradiance is also highly sensitive to early stage quantum fluctuations.

Since ensemble averages of atomic observables are experimentally measurable quantities, we consider these in
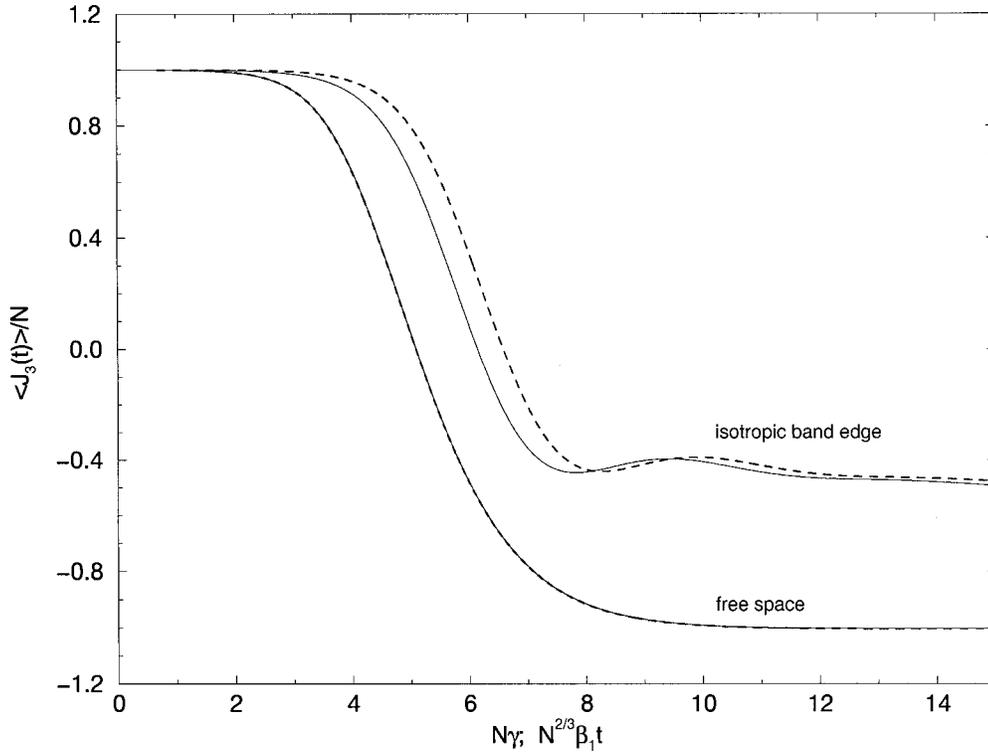
FIG. 10. Atomic inversion for superradiance driven by vacuum fluctuations in free space and for an atomic resonant frequency tuned to an isotropic photonic band edge ($\delta_c = 0$). Solid lines, result for initial polarization distribution at $t = 0$ for each system; dashed lines, result for initial polarization distribution at $t = t_0$ for each system.

some detail. We use the notation $\langle \rangle_{\mathrm{ens}}$ to denote an ensemble-averaged quantum expectation value. For illustration, we focus on the $\delta_c = 0$ and zero dephasing case for a system of 100 atoms in the isotropic effective-mass model. The extension to non-zero detuning and finite dipole dephasing follows from the discussion of Sec. IV. From Fig. 11, it is evident that the ensemble exhibits a fractional population inversion in the steady state. The steady-state value of

$\langle J_3(t) \rangle_{\mathrm{ens}}$ for a given atomic detuning is unchanged from the mean-field result, $\langle J_3(t_s) \rangle$. Since the steady state is determined by the atom-field coupling strength, and not by the dynamics of the system, it is insensitive to initial conditions. Fluctuations in the excited-state atomic population may be expressed in terms of the delay time for the onset of superradiant emission, defined as the time at which the system is exactly half excited, i.e., $\langle J_3 \rangle = 0$. Vacuum fluctuations result in a distribution of delay times for the ensemble, asymmetrically centered about a peak value, as pictured in Fig. 12. The delay time distribution is qualitatively similar to that ob-
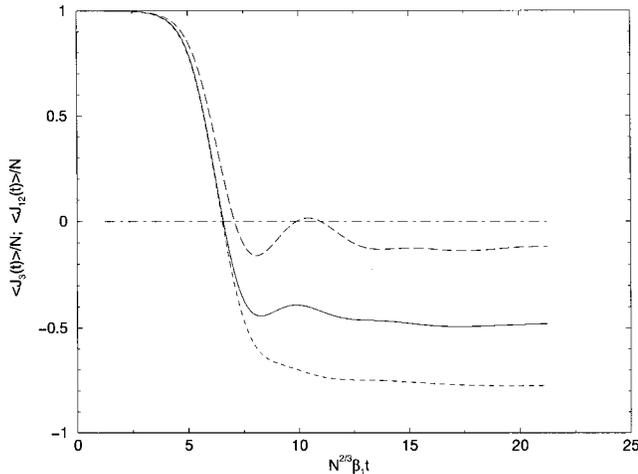

FIG. 11. Ensemble-averaged atomic inversion, $\langle J_3(t) \rangle_{\mathrm{ens}}/N$, and atomic polarization amplitude, $|\langle J_{12}(t) \rangle_{\mathrm{ens}}|/N$ (dot-dashed line), for a system of $N = 100$ atoms near an isotropic photonic band edge. The ensemble average is taken over 2000 initial polarization values. Inversion: long-dashed curve, $\delta_c = -0.5$; solid line, $\delta_c = 0$; short-dashed line, $\delta_c = 0.5$. δ_c in units of $N^{2/3}\beta_1$.
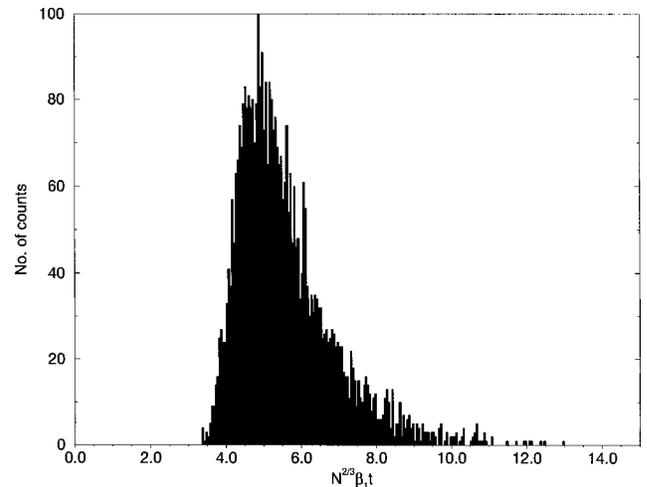

FIG. 12. Distribution of delay times for a system of 100 atoms at an isotropic band edge ($\delta_c = 0$) for 4000 realizations of the superradiant system.
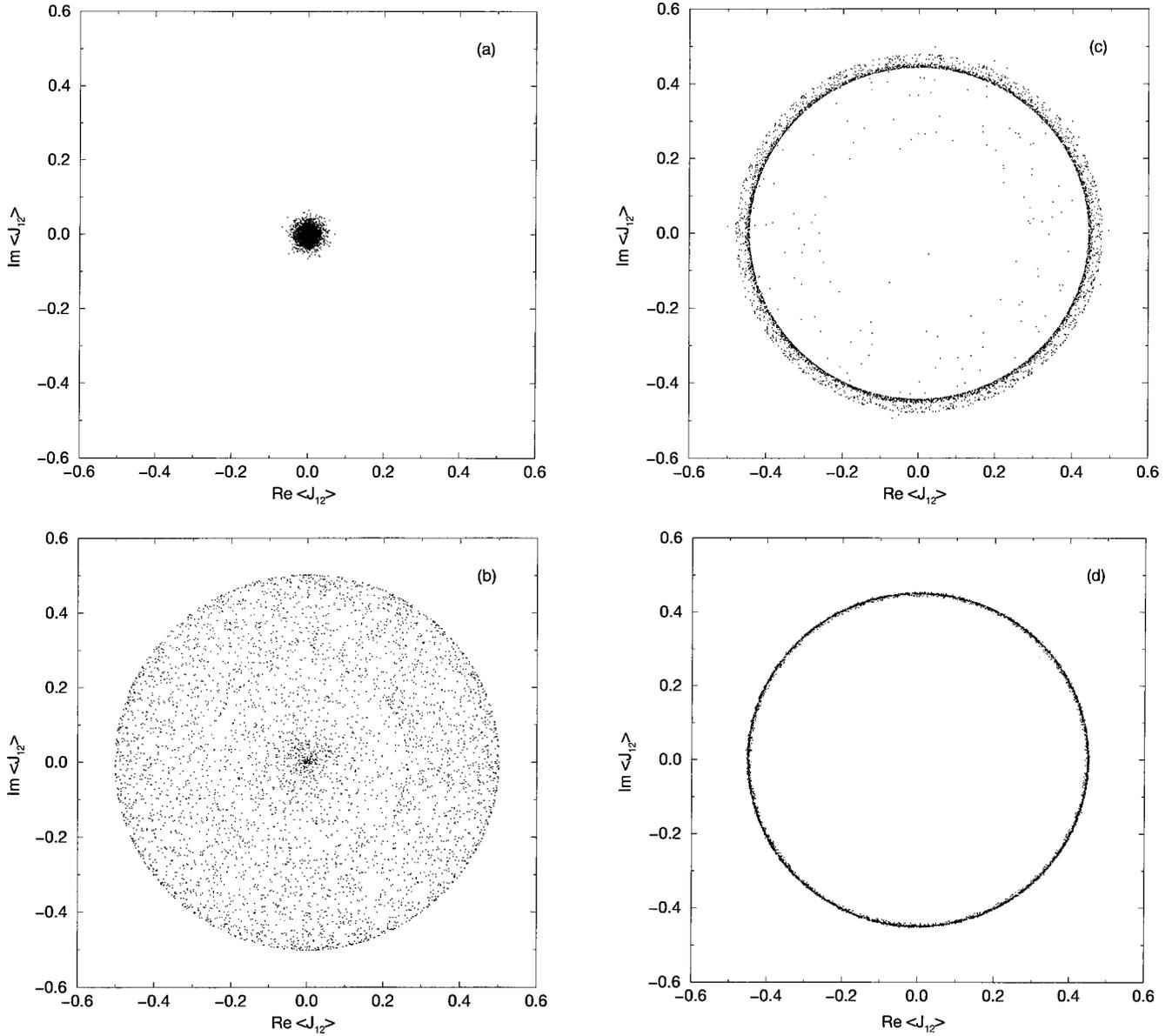
FIG. 13. Atomic polarization distribution for a system of 100 atoms at an isotropic band edge ($\delta_c = 0$), subject to quantum fluctuations at early times. 5000 realizations of the superradiant system. (a) $t = t_0^{\mathrm{PBG}}$; (b) $t = 5$; (c) $t = 11$; (d) steady state. t in units of $1/N^{2/3}\beta_1$.

tained in free space [33]. However, the width of the distribution scales with the relevant time scale for the isotropic and anisotropic gaps, showing that, near a photonic band edge, atomic population fluctuations during light emission can be reduced from their free space value. Because of the variation in initial conditions, the Rabi oscillations in $\langle J_3(t)\rangle$ for the isotropic gap are much less pronounced than in mean-field simulations. The differences in emission times due to fluctuations cause the ensemble average inversion to smear out these oscillations. Therefore, one can no longer directly relate the amplitude and period of the oscillations to the energies of the collective dressed states.

More striking is the nature of the ensemble's collective polarization under the influence of vacuum fluctuations. Figures 13(a)–13(d) show the evolution of the polarization distribution from the initial distribution given by Eqs. (5.17) and (5.19) to the steady-state distribution. Initially, the distribution is sharply peaked about zero. In the decay region, the polarization amplitude is broadly distributed and has a

random phase. This behavior is reminiscent of the fluctuations of the order parameter in the vicinity of a phase transition. In the steady state, the polarization amplitude collapses to a very well-defined nonzero value. This amplitude is again accompanied by a random phase that is uniformly distributed between 0 and 2π. We may interpret our steady-state result in the following manner: A fraction of the photons emitted near the photonic band edge remain localized in the vicinity of the atoms, causing both the atomic dipoles and the electromagnetic field to self-organize into a cooperative steady state. However, vacuum fluctuations cause this cooperative quantum state to have a random phase, resulting in a zero ensemble average polarization amplitude, $|\langle J_{12}(t)\rangle_{\mathrm{ens}}| = 0$, as shown in Fig. 11. Measurements of the degree of first- and second-order coherence of the electromagnetic field in a band-edge superradiance experiment would provide a probe of the nature of this self-organized state of photons and atoms near a band edge. We further note that this state—well defined in amplitude but

with random phase—is similar to the steady state of a conventional laser [34] with a well-defined electric field amplitude and random phase diffusion.

VI. SIMULATED QUANTUM NOISE NEAR A BAND EDGE

We have shown that the statistical properties of a band-edge superradiant system can be determined because the collective behavior of the constituent atoms leads to a semiclassical system evolution, triggered by early-time quantum fluctuations. However, a seamless quantum description of band-edge quantum optical systems is extremely difficult to obtain, due to the non-Markovian nature of the atom-field interaction. As a first step, we introduce a method by which to simulate their evolution computationally and include the effects of quantum fluctuations. Unlike the semiclassical simulations of Sec. IV, which neglected the effect of the quantum noise operator, as $\langle \eta(t) \rangle = \langle \eta^\dagger(t) \rangle = 0$, we propose to replace $\langle \eta(t) \rangle$ in our semiclassical equations by a complex classical stochastic function with the same mean and two-time correlation function as its quantum counterpart. This noise function then simulates the quantum noise in our system throughout the entire system evolution. We may test the validity of our simulated noise ansatz for band-edge superradiance by comparing the results obtained to those calculated in Sec. V.

The classical noise function required to simulate quantum noise near a photonic band edge involves a real stochastic function $\xi(t)$ possessing the underlying temporal autocorrelation of our non-Markovian quantum noise operator, $\eta(t)$. In the effective-mass approximation, this means that [see Eqs. (2.10) and (2.11)],

$$\langle \xi(t)\xi(t') \rangle = \frac{1}{(t-t')^{\alpha/2}}, \qquad (6.1)$$

where again $\alpha = 1$ and 3 for isotropic and anisotropic band edges, respectively. Problems in band-edge atom-field dynamics, such as the present superradiant problem, often involve nonlinear equations under the influence of colored quantum noise. It is interesting to note that nonlinear problems involving classical colored noise are of considerable interest in classical statistical physics [35]. In what follows, we use the method first introduced by Rice [36] and elaborated on by Billah and Shinozuka [37] in order to generate colored noise satisfying Eq. (6.1). For noise with a power spectrum $P(\omega)$, defined as the Fourier transform of the autocorrelation function $\langle \xi(t)\xi(t') \rangle$, their algorithm gives

$$\xi(t) \simeq 2\sum_{n=1}^{N} [P(\omega_n)\Delta\omega]^{1/2}\cos(\omega_n t + \Phi_n), \quad n=1,2,\dots,N,$$
$$(6.2)$$

with equality obtained for $N \to \infty$. Here, $\omega_n = n\Delta\omega$, $\Delta\omega = \omega_{max}/N$, and ω_{max} is a cutoff frequency above which the power spectrum can be neglected. Each Φ_n is a random phase uniformly distributed in the range $[0,2\pi]$. By use of a particular set of random phases $\{\Phi_n\}$ to generate the noise values at each time step, we obtain a single ''experimental'' realization of the quantum noise in our system. Since we cannot predict *a priori* the specific form of the quantum fluctuations in a particular experiment, we again average over many realizations of the superradiant system, each governed by a different $\xi(t)$, in order to obtain distributions and ensemble averages of relevant quantities. We note that Eq. (6.2) clearly gives $\langle \xi(t) \rangle_{ens} = 0$, as desired, since the random Φ_n cause the ensemble to average to zero. To show that Eq. (6.2) also gives the correct autocorrelation function, we write

$$\langle \xi(t)\xi(t') \rangle_{ens} = \left\langle 4\Delta\omega\sum_{k}\sum_{l} [P(\omega_k)P(\omega_l)]^{1/2}\cos(\omega_k t + \Phi_k)\cos(\omega_l t' + \Phi_l) \right\rangle_{ens}$$

$$= \left\langle 2\Delta\omega\sum_{k}\sum_{l} [P(\omega_k)P(\omega_l)]^{1/2}\{\cos(\omega_k t - \omega_l t' + \Phi_k - \Phi_l) + \cos(\omega_k t + \omega_l t' + \Phi_k + \Phi_l)\} \right\rangle_{ens} \qquad (6.3)$$

$$= \left\langle 2\Delta\omega\sum_{k} P(\omega_k)\cos[\omega_k(t-t')] \right\rangle_{ens}. \qquad (6.4)$$

In Eq. (6.3), only the $k=l$ components, in which the random phases Φ_k and Φ_l cancel each other, survive the ensemble average. As $N \to \infty$, Eq. (6.4) becomes the Fourier transform of $P(\omega)$, which equals $\langle \xi(t)\xi(t') \rangle_{ens}$. Studies have shown that for values of N as small as 1000, the desired autocorrelation may be obtained with as little as 5% error [37], making this a computationally feasible technique. Furthermore, unlike other methods for the generation of stochastic functions (see Ref. [35]), the present method computes the desired function, $\xi(t)$, using only a uniform random distribu-

tion of phases Φ_k as input, rather than requiring the computation of a Gaussian stochastic function as an intermediate step. This decreases the likelihood of spurious correlations between our random numbers. Figure 14 shows the two-time correlation of $\xi(t)$ for $\alpha = 1$, for an ensemble of 2000 realizations of the noise function generated by the algorithm of Eq. (6.2). In this calculation and in the simulations described below, we chose a power spectrum $P(\omega) = \sqrt{\pi/2\omega}$, in order to mimic the colored vacuum near an isotropic band edge. We see good agreement with the corre-
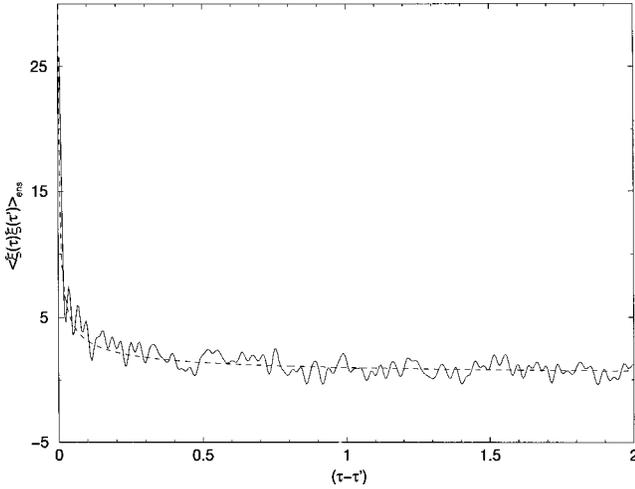
FIG. 14. Solid line: ensemble-averaged autocorrelation function, $\langle \xi(\tau)\xi(\tau')\rangle_{\text{ens}}$, of the classical colored noise function $\xi(\tau)$ corresponding to vacuum fluctuations near an isotropic band edge. The dashed line is a plot of the exact autocorrelation function in the effective-mass approximation, $(\tau-\tau')^{-1/2}$.

FIG. 15. Comparison of the ensemble averaged atomic inversion, $\langle J_3(t)\rangle_{\text{ens}}/N$, at an isotropic band edge ($\delta_c=0$) as calculated by the methods of Secs. V and VI. 2000 realizations of the superradiant system. Dashed line and double dashed line, inversion calculated using the computed polarization distribution at $t=t_0^{\text{PBG}}$ as initial conditions for a semiclassical evolution (Sec. V) for $N=1000$ and 10 000 atoms, respectively. Solid line and dotted lines, inversion calculated using the stochastic function of Sec. VI for $N=1000$ and 10 000 atoms, respectively.

lation function (6.1). The agreement between our simulations and the exact correlation function can be significantly improved by enlarging the size of the ensemble, at the expense of increased computation time for atom-field simulations.

The ensemble $\{\xi(t)\}$ is used to simulate the effect of vacuum fluctuations in Eqs. (2.5) and (2.6). Written in terms of the dimensionless time variable $\tau=N^{2/3}\beta_1 t$, these equations for the isotropic band edge become

$$\frac{d}{d\tau}\langle J_3(\tau)\rangle$$

$$= -4\,\text{Re}\Bigg\{ e^{-i\pi/4}\frac{\langle J_{21}(\tau)\rangle}{\sqrt{\pi}}\int_0^\tau \frac{\langle J_{21}(\tau')\rangle}{\sqrt{\tau-\tau'}}e^{i\delta_c(\tau-\tau')}d\tau'$$

$$+ \frac{\langle J_{21}(\tau)\rangle e^{-i(\pi/8-\delta_c\tau)}}{\sqrt{N\sqrt{\pi}}}\xi(\tau)\Bigg\}, \tag{6.5}$$

$$\frac{d}{d\tau}\langle J_{12}(\tau)\rangle = e^{-i\pi/4}\frac{\langle J_3(\tau)\rangle}{\sqrt{\pi}}\int_0^\tau \frac{\langle J_{21}(\tau')\rangle}{\sqrt{\tau-\tau'}}e^{i\delta_c(\tau-\tau')}d\tau'$$

$$+ \frac{\langle J_3(\tau)\rangle e^{-i(\pi/8-\delta_c\tau)}}{\sqrt{N\sqrt{\pi}}}\xi(\tau), \tag{6.6}$$

with similar equations for the anisotropic gap. For both models, the noise term scales as $1/\sqrt{N}$; this is the same dependence of the noise term on particle number exhibited in free space [32]. In Fig. 15, we show the average inversion for an ensemble containing 2000 realizations of $\xi(\tau)$ for $N=1000$ and $N=10\,000$ atoms. We find that our stochastic simulation scheme gives physical results only for systems of $N>500$ atoms. The stochastic simulations show good agreement with the atomic inversion obtained by the method of Sec. V. Other system properties, such as the ensemble-
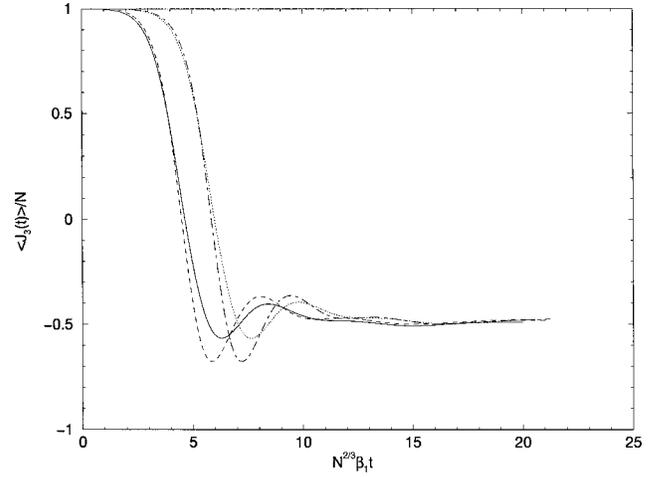
averaged polarization and the delay time distribution calculated by the present method also agree well with the quantum calculations of the previous section. This suggests that our stochastic approach may be a valuable tool in the analysis of band-edge atom-field dynamics.

VII. CONCLUSIONS

In this paper, we have treated the collective spontaneous emission of two-level atoms near a photonic band edge. An analytic calculation of the atomic operator dynamics in the case of low atomic excitation was given. The results demonstrate highly atypical atomic emission spectra and show the possibility of reducing atomic population fluctuations. This in turn suggests that fluctuations in photon number are likewise suppressed for light localized near the atoms. This raises the interesting question of whether squeezed light [38], antibunched photons [39], and other forms of nonclassical light may be generated in a simple manner from band edge atom-field systems. For an initially inverted system prepared with a small macroscopic polarization, a mean field factorization was applied to the atomic quantum Langevin equations, giving a semiclassical system evolution. We found that the atoms exhibit fractional population trapping and a macroscopic polarization in the steady state. Collective Rabi oscillations of the atomic population were found, and were attributed to the interference of strongly dressed atom-photon states that are repelled from the band edge, both into and out of the gap. The degree of photon localization, the polarization amplitude, and the phase angle of the polarization in the steady state are all sensitive functions of the detuning of the atomic resonant frequency from the band edge. The steady-state atomic properties can thus be controlled by applying a dc Stark shift to the atomic resonant frequency. In Sec. IV, we discussed the effect on band-edge superradiance of inter-

atomic and atom-phonon interactions (atomic dephasing). We showed that such linewidth broadening effects cannot be treated by a phenomenological decay constant as in free space, and that near the band edge they will lead to the decay of atomic polarization and inversion. Therefore, the steady-state properties of the superradiant system described in this paper will be limited by the time scale of the atomic dephasing effects. The effect of dephasing mechanisms is important to the description of almost all band edge atom-field systems. As a particular example, dephasing determines the threshold external pumping required to achieve atomic inversion in a laser operating near a photonic band edge. It also facilitates the emission of laser light from a photonic crystal.

The effect of quantum fluctuations for high initial excitation of the atoms was included by distinguishing regimes of quantum and semiclassical collective atomic evolution. We found that the early time quantum evolution must be treated in detail, due to the non-Markovian electromagnetic reservoir correlations near a band edge. This is in contrast with free space, where the atomic system's evolution is insensitive to the treatment of the full temporal evolution of the early, quantum regime. Fractional localization of light was shown to persist under the influence of vacuum fluctuations. The atomic polarization exhibits a nonzero amplitude with a randomly distributed phase in the steady state. This is much like the steady state of a conventional laser. Here, such lasing characteristics are due only to the Bragg scattering of photons back to the atoms; there is neither external pumping nor a laser cavity in our system. The time scales for all dynamical processes, such as collective emission and the buildup of collective atomic polarization are strongly modified from their free space values due to the singular photon density of states near a photonic band edge. For an isotropic band edge, the time scales as $N^{2/3}\beta_1$, while in the more realistic anisotropic model, time scales as $N^2\beta_3$. As a result, collective emission phenomena can occur more rapidly near a band edge than in free space. Throughout our calculations, we have employed an effective-mass approximation to the band-edge dispersion. For materials with a very small PBG, it may be important to include the effects of both band edges. These issues are raised in Appendix A.

We have demonstrated that band-edge superradiance possesses many of the self-organization and coherence properties of a conventional laser. Furthermore, we have shown the possibility for the generation of unusual emission spectra and photon statistics. These results suggest that a laser operating near a photonic band edge may possess unusual spectral and statistical properties, as well as a low input power lasing threshold due to the fractional inversion of the atoms in the steady state. It may further be possible to produce a PBG laser in a bulk material without recourse to a defect-induced cavity mode. Lending credence to this hypothesis, recent observations [40] and theoretical studies [41] of lasing from a multiply scattering random medium with gain have demonstrated that one may obtain light with the properties of a laser field in the absence of a cavity. A full description of the statistics of a band-edge laser field will require a treatment of the non-Markovian nature of the electromagnetic reservoir. Current techniques for treating the atom-field interaction in the absence of the Born and Markov approximations [42,43] cannot account for the van Hove singularity in the density of states encountered at a photonic band edge, nor are they all directly applicable to externally driven atomic systems.

Finally, we note that the steady state atom-field properties described here are a result of the effect of radiation localized in the vicinity of the active two-level atoms. This leads to the question of how to pump energy into and extract energy out of these states, which lie within the forbidden photonic gap. One possibility is to couple energy into and/or out of the system through a third atomic level whose transition energy lies outside the gap [15]. There is also the possibility of transmitting light into the gap through high intensity ultrashort pulses that locally distort the nonlinear dielectric constant of the material and thus allow the propagation of light in the form of solitary waves within the forbidden frequency range [44]. Such issues must be addressed in order to fully exploit the very rich possibilities of quantum optical processes near a photonic band edge.

APPENDIX A: CALCULATION OF THE MEMORY KERNEL

We first present the calculation of the memory kernel for the isotropic model in the effective-mass approximation, $G_I(t-t')$. Starting from Eq. (2.8) and the isotropic dispersion relation near the upper band edge, $\omega_k = \omega_c + A(|\mathbf{k}| - |\mathbf{k}_0|)^2$, $G_I(t-t')$ can be expressed as

$$G_I(t-t') = \frac{\omega_{21}^2 d_{21}^2}{4\hbar\epsilon_0\pi} e^{i\delta_c(t-t')} \int d\Omega \int_{k_0}^{\Lambda} dk \frac{e^{-iA(k-k_0)^2(t-t')}}{\omega_c + A(k-k_0)^2}. \tag{A1}$$

Again, $\delta_c = \omega_{21} - \omega_c$ is the detuning of the atomic resonant frequency from the band edge. $\Lambda = mc/\hbar$ is a cutoff in the photon wave vector above the electron rest mass. Photons of energy higher than the electron rest mass probe the relativistic structure of the electron wave packets of our resonant atoms [45]. Because the isotropic model associates the band edge with a sphere in k space, there is no angular dependence in the expansion of $\omega_\mathbf{k}$ about the band edge. We may thus separate out the angular integration over solid angle Ω in Eq. (A1). We may also make a stationary phase approximation to the integral, as the nonexponential part of the integrand will only contribute significantly to the integral for $k \simeq k_0$. The resulting integral is

$$G_I(t-t') \simeq \frac{\omega_{21}^2 d_{21}^2}{4\hbar\epsilon_0\pi} \frac{k_0}{\omega_c} e^{i\delta_c(t-t')} \int_{k_0}^{\Lambda} dk\, e^{-iA(k-k_0)^2(t-t')}. \tag{A2}$$

As Λ is a large number, we extend the range of integration to infinity in order to obtain a simple analytic expression for $G_I(t-t')$ [46]:

$$G_I(t-t') = \frac{\omega_{21}^2 \omega_c \sqrt{\omega_{\text{gap}}} d_{21}^2}{12\hbar\,\epsilon_0\pi^{3/2}c^3} \frac{e^{-i[\pi/4-\delta_c(t-t')]}}{\sqrt{t-t'}}$$

$$= \beta_1^{3/2} \frac{e^{-i[\pi/4-\delta_c(t-t')]}}{\sqrt{t-t'}}. \tag{A3}$$

Because the relevant frequencies in Eq. (A3) are roughly of the same order of magnitude near a band edge, we may rewrite the prefactor as $\beta_1^{3/2} \simeq \omega_{21}^{7/2}d_{21}^2/12\hbar\,\epsilon_0\pi^{3/2}c^3$, in agreement with the value given in Sec. II. We emphasize that the stationary phase method yields the correct asymptotic behavior for the memory kernel for large $|t-t'|$. At short times, the integral must be evaluated more precisely using the full photon dispersion relation, as discussed below.

For an anisotropic band-gap model, we must account for the variation in the magnitude of the band-edge wave vector as $\mathbf{k}$ is rotated throughout the Brillouin zone. We associate the gap with a specific point in k space that satisfies the Bragg condition, $\mathbf{k}=\mathbf{k}_0$. In the effective-mass approximation, the dispersion relation is expanded to second order in k about this point, $\omega_{\mathbf{k}}=\omega_c\pm A(\mathbf{k}-\mathbf{k}_0)^2$. Making the substitution $\mathbf{q}=\mathbf{k}-\mathbf{k}_0$ and performing the angular integration, $G_A(t-t')$ is expressed as

$$G_A(t-t') = \frac{\omega_{21}^2 d_{21}^2}{4\hbar\,\epsilon_0\pi^2} e^{i\delta_c(t-t')} \int_0^\Lambda dq\, \frac{q^2 e^{-iAq^2(t-t')}}{\omega_c+Aq^2}. \tag{A4}$$

Extending the wave-vector integration to infinity, the Green function is [46]

$$G_A(t-t') = \frac{\omega_{21}^2 d_{21}^2}{8\hbar\,\epsilon_0\pi^2} e^{i\delta_c(t-t')}\left\{ \sqrt{\frac{\pi}{i\omega_c(t-t')}} - \frac{\pi}{2}\sqrt{\frac{\omega_c}{A}} e^{i\omega_c(t-t')}[1-\Phi(\sqrt{i\omega_c(t-t')})] \right\}. \tag{A5}$$

$\Phi(x)$ is the probability integral, $\Phi(x)=(2/\sqrt{\pi})\int_0^x e^{-t^2}dt$. For $\omega_c(t-t')\gg 1$, a condition satisfied for all but the $t'\to t$ limit (as $\omega_c\sim 10^{15}$ s^{-1} for optical transitions), taking the asymptotic expansion of $\Phi(x)$ to second order gives

$$G_A(t-t') = \frac{\omega_{21}^2 d_{21}^2}{8\hbar\,\epsilon_0(\pi A)^{3/2}\omega_c} \frac{e^{i[\pi/4+\delta_c(t-t')]}}{(t-t')^{3/2}},$$

$$\omega_c(t-t')\gg 1. \tag{A6}$$

As $t-t'\to 0_+$, Eq. (A5) reduces to

$$G_A(t-t') = \frac{\omega_{21}^2 d_{21}^2}{8\hbar\,\epsilon_0\pi^2 A^{3/2}}\left[\sqrt{\frac{\pi}{i\omega_c(t-t')}} - \pi\sqrt{\omega_c} \right],$$

$$t-t'\to 0_+. \tag{A7}$$

$G_A(t-t')$ possesses a weak (square root) singularity at $t=t'$. This is an integrable singularity and can thus be treated numerically [47].

The effective-mass dispersion relation used in the evaluation of $G(t-t')$ is, strictly speaking, valid only near the photonic band edge, as it fails to give the required linear photon dispersion relation for large $|k-k_0|$ (far away from the gap). Therefore, the integration of the effective-mass dispersion for large wave vector in Eqs. (A1) and (A4) introduces a spurious contribution to $G(t-t')$. This difficulty may be overcome for an isotropic gap model by using a dispersion relation that has the correct wave-vector dependence for all k. The simplest model dispersion with the correct form is

$$\omega_k/c = \sqrt{k_0^2+\gamma^2} + \text{sgn}(k-k_0)\sqrt{(k-k_0)^2+\gamma^2}. \tag{A8}$$

The double-valued nature of ω_k at k_0 is made explicit by the function $\text{sgn}(k-k_0)=1$ for $k>k_0$, and $\text{sgn}(k-k_0)=-1$ for $k<k_0$. This gives a gap of width $\omega_{\text{gap}}=2\gamma c$, centered about the midgap frequency $\omega_0=c\sqrt{k_0^2+\gamma^2}$. Note that Eq. (A8) gives the correct linear dependence in k for both large positive and negative k, and gives the effective-mass dispersion for $k\sim k_0$. Like the effective-mass model, Eq. (A8) gives a singular density of states at the band edges, $\omega_c=\omega_0\pm c\gamma$. The full dispersion relation allows us to evaluate the influence of both band edges for arbitrary gap width and atomic resonant frequency. Preliminary numerical calculations show a stronger reservoir memory effect than demonstrated in the effective mass model for the isotropic band edge. This may have a significant effect on theoretical predictions regarding the atom-field interaction in the vicinity of a PBG. A further simplification has been made in the anisotropic model, in that we have not included the dependence of $\omega_{\mathbf{k}}$ on the symmetry of a specific photonic crystal. In a real three-dimensional PBG material, the Bragg condition is satisfied for different values of $\mathbf{k}$ as the wave vector changes direction in k space. This directional dependence may lead to a much stronger dependence of the localization of light on the detuning of ω_{21} away from the band edge. The impact on the atom-field interaction in a PBG of both the full isotropic dispersion model and more realistic dispersions for three-dimensional photonic crystals will be treated elsewhere.

APPENDIX B: EVALUATION OF $\Sigma_\lambda|A_\lambda(t)|^2$

We outline the evaluation of $\Sigma_\lambda|A_\lambda(t)|^2$, used to obtain the low excitation population fluctuations in Sec. III, Eq. (3.19). A similar procedure is used to arrive at Eq. (5.12) in Sec. V. Starting from the Laplace transform $\tilde{A}_\lambda(s)$ [Eq.

(3.7)], we may use the properties of a convolution of Laplace transforms in order to write

$$A_\lambda(t) = g_\lambda \int_0^t dt' B(t') e^{-i\Delta_\lambda t}. \quad \text{(B1)}$$

Therefore, we have

$$\sum_\lambda |A_\lambda(t)|^2 = \int_0^t dt' \int_0^t dt'' B(t'') B^*(t') G(t'-t''), \quad \text{(B2)}$$

with $G(t-t')$ defined as in Eq. (2.7). We may rewrite this double integral in the form

$$\sum_\lambda |A_\lambda(t)|^2 = \int_0^t dt' \int_0^{t'} dt'' B(t'') B^*(t') G(t'-t'')$$
$$+ \int_0^t dt' \int_{t'}^t dt'' B(t'') B^*(t') G(t'-t'')$$
$$= I_1 + I_2, \quad \text{(B3)}$$

where I_1 and I_2 are the first and second double integrals, respectively. By changing the order of the integrations in I_2, we obtain

$$I_2 = \int_0^t dt'' \int_0^{t''} dt' B(t'') B^*(t') G(t'-t'') = I_1^*. \quad \text{(B4)}$$

Therefore, $\Sigma_\lambda |A_\lambda(t)|^2 = 2 \, \text{Re}\{I_1\}$, and we need only explicitly evaluate I_1. The Laplace transform of $B(t)$, $\widetilde{B}(s)$ [Eq. (3.6)], is equivalent to the Laplace transform of the equation

$$\frac{d}{dt} B(t) = -N \int_0^t dt' G(t-t') B(t'). \quad \text{(B5)}$$

Substituting Eq. (B5) into I_1 and its complex conjugate, we obtain

$$2I_1 = -\frac{1}{N} \int_0^t dt' \, \frac{d}{dt'} |B(t')|^2$$
$$= \frac{1}{N} [|B(0)|^2 - |B(t)|^2] = \sum_\lambda |A_\lambda(t)|^2, \quad \text{(B6)}$$

as I_1 is real. Substituting the initial condition $|B(0)|^2 = 1$ into Eq. (B6) gives the result quoted in Sec. III.

[1] S. John, Phys. Rev. Lett. **53**, 2169 (1984).
[2] S. John, in *Photonic Bandgap Materials*, edited by C. M. Soukoulis, Vol. 315 of *NATO Advanced Studies Institute Series E* (Kluwer Academic, Dordrecht, 1996).
[3] E. Yablonovich, Phys. Rev. Lett. **58**, 2059 (1987).
[4] S. John, Phys. Rev. Lett. **58**, 2486 (1987).
[5] E. Yablonovich, T. J. Gmitter, and K. M. Leung, Phys. Rev. Lett. **67**, 2295 (1991).
[6] U. Grüning, V. Lehman, S. Ottow, and K. Busch, Appl. Phys. Lett. **68**, 747 (1996).
[7] W. L. Vos, R. Sprik, A. van Blaaderen, A. Imhof, A. Lagendijk, and G. H. Wegdam, Phys. Rev. B **53**, 16 231 (1996).
[8] V. N. Bogomolov, S. V. Gaponenko, I. N. Germanenko, A. M. Kapitonov, E. P. Petrov, N. V. Gaponenko, A. V. Prokofiev, A. N. Ponyavina, N. I. Silvanovich, and S. M. Samoilovich, Phys. Rev. E **55**, 7619 (1997).
[9] H. Míguez, C. López, F. Meseguer, A. Bianco, L. Vázquez, R. Mayoral, M. Ocaña, V. Fornés, and A. Mifsud, Appl. Phys. Lett. **71**, 1148 (1997).
[10] Yu. A. Vlasov, K. Luterova, I. Pelant, B. Hönerlage, and V. N. Astratov, Appl. Phys. Lett. **71**, 1616 (1997).
[11] S. John and J. Wang, Phys. Rev. Lett. **64**, 2418 (1990); Phys. Rev. B **43**, 12 772 (1991).
[12] Y. Yamamoto and R. E. Slusher, Phys. Today **46** (6), 66 (1993).
[13] W. H. Louisell, *Quantum Statistical Properties of Radiation* (Wiley, New York, 1973).
[14] R. F. Nabiev, P. Yeh, and J. J. Sanchez Mondragon, Phys. Rev. A **47**, 3380 (1993).
[15] S. John and T. Quang, Phys. Rev. A **50**, 1764 (1994).
[16] R. Dicke, Phys. Rev. **93**, 493 (1954).
[17] M. Gross and S. Haroche, Phys. Rep. **93**, 301 (1982).
[18] F. Haake, M. I. Kolobov, C. Fabre, E. Giacobino, and S. Reynaud, Phys. Rev. Lett. **71**, 995 (1993).
[19] R. G. DeVoe and R. G. Brewer, Phys. Rev. Lett. **76**, 2049 (1996).
[20] S. John and T. Quang, Phys. Rev. Lett. **74**, 3419 (1995).
[21] S. John and T. Quang, Phys. Rev. Lett. **76**, 1320 (1996).
[22] S. John and V. Rupasov, Phys. Rev. Lett. **79**, 821 (1997).
[23] J. Schwinger, in *Quantum Theory of Angular Momentum*, edited by L. C. Biedenharn (Academic Press, New York, 1965).
[24] L. Mandel, Opt. Lett. **4**, 205 (1979).
[25] S. Bay, P. Lambropoulos, and K. Mølmer, Phys. Rev. A **57**, 3065 (1998).
[26] Y. Kaluzny, P. Goy, M. Gross, J. M. Raimond, and S. Haroche, Phys. Rev. Lett. **51**, 1175 (1983).
[27] L. Allen and J. H. Eberly, *Optical Resonance and Two-Level Atoms* (Dover, New York, 1987).
[28] M. Woldeyohannes and S. John (unpublished).
[29] D. Deutsch, Proc. R. Soc. London, Ser. A **400**, 96 (1985); A. Barenco, D. Deutsch, A. Ekert, and R. Jozsa, Phys. Rev. Lett. **74**, 4083 (1995); T. Sleator and H. Weinfurter, Phys. Rev. Lett. **74**, 4087 (1995); J. I. Cirac and P. Zoller, *ibid.* **74**, 4091 (1995).
[30] T. Quang, M. Woldeyohannes, S. John, and G. Agarwal, Phys. Rev. Lett. **79**, 5238 (1997).
[31] P. Meystre and M. Sargent, *Elements of Quantum Optics* (Springer-Verlag, New York, 1991).
[32] D. Polder, M. F. H. Schurmans, and Q. H. F. Vrehen, Phys. Rev. A **19**, 1192 (1979).
[33] F. Haake, H. King, G. Schröder, J. Haus, and R. Glauber, Phys. Rev. A **20**, 2047 (1979).
[34] M. Sargent, M. O. Scully, and W. E. Lamb, *Laser Physics*

(Addison-Wesley, New York, 1974).

[35] A. Barabasi, *Fractal Concepts in Surface Growth* (Cambridge University Press, New York, 1995); E. Medina, T. Hwa, M. Kardar, and Y. Zhang, Phys. Rev. A **39**, 3053 (1989); C. Peng, S. Havlin, M. Schwartz, and H. E. Stanley, Phys. Rev. A **44**, R2239 (1991).

[36] S. O. Rice, in *Selected Papers on Noise and Stochastic Processes*, edited by N. Wax (Dover, New York, 1954).

[37] K. Y. R. Billah and M. Shinozuka, Phys. Rev. A **42**, 7492 (1990), and references therein.

[38] D. F. Walls, Nature (London) **306**, 141 (1983).

[39] R. Loudon, *The Quantum Theory of Light*, 2nd ed. (Oxford University Press, Oxford, 1983).

[40] N. M. Lawandy, R. M. Balachandran, A. S. L. Gomes, and E. Sauvain, Nature (London) **368**, 436 (1994).

[41] S. John and G. Pang, Phys. Rev. A **54**, 3642 (1996).

[42] A. Imamoglu, Phys. Rev. A **50**, 3650 (1994).

[43] B. M. Garraway, Phys. Rev. A **55**, 2290 (1997).

[44] S. John and N. Aközbek, Phys. Rev. Lett. **71**, 1168 (1993); N. Aközbek and S. John, Phys. Rev. E **57**, 2287 (1998).

[45] H. A. Bethe, Phys. Rev. **72**, 339 (1947).

[46] I. S. Gradshteyn and I. M. Ryzhik, *Table of Integrals, Series and Products* (Academic Press, New York, 1980).

[47] P. J. Davis and P. Rabinowitz, *Methods of Numerical Integration*, 2nd ed. (Academic Press, New York, 1984).